nature metabolism

ARTICLES

https://doi.org/10.1038/s42255-020-00288-1

Check for updates

Mitochondrial pyruvate carriers are required for myocardial stress adaptation

Yuan Zhang[1,2], Paul V. Taufalele[1], Jesse D. Cochran[1], Isabelle Robillard-Frayne[3], Jonas Maximilian Marx[4,5], Jamie Soto[1,6], Adam J. Rauckhorst[1], Fariba Tayyari[7], Alvin D. Pewa[7], Lawrence R. Gray[1], Lynn M. Teesch[7], Patrycja Puchalska[4,8], Trevor R. Funari[1], Rose McGlauflin[1], Kathy Zimmerman[9], William J. Kutschke[9], Thomas Cassier[1], Shannon Hitchcock[1], Kevin Lin[1], Kevin M. Kato[1], Jennifer L. Stueve[1], Lauren Haff[1], Robert M. Weiss[9], James E. Cox[10,11], Jared Rutter[10,12], Eric B. Taylor[1,7,13], Peter A. Crawford[4,8], E. Douglas Lewandowski[4,14], Christine Des Rosiers[3] and E. Dale Abel[1,2,9] ✉

In addition to fatty acids, glucose and lactate are important myocardial substrates under physiologic and stress conditions. They are metabolized to pyruvate, which enters mitochondria via the mitochondrial pyruvate carrier (MPC) for citric acid cycle metabolism. In the present study, we show that MPC-mediated mitochondrial pyruvate utilization is essential for the partitioning of glucose-derived cytosolic metabolic intermediates, which modulate myocardial stress adaptation. Mice with cardiomyocyte-restricted deletion of subunit 1 of MPC (cMPC1$^{-/-}$) developed age-dependent pathologic cardiac hypertrophy, transitioning to a dilated cardiomyopathy and premature death. Hypertrophied hearts accumulated lactate, pyruvate and glycogen, and displayed increased protein O-linked *N*-acetylglucosamine, which was prevented by increasing availability of non-glucose substrates in vivo by a ketogenic diet (KD) or a high-fat diet, which reversed the structural, metabolic and functional remodelling of non-stressed cMPC1$^{-/-}$ hearts. Although concurrent short-term KDs did not rescue cMPC1$^{-/-}$ hearts from rapid decompensation and early mortality after pressure overload, 3 weeks of a KD before transverse aortic constriction was sufficient to rescue this phenotype. Together, our results highlight the centrality of pyruvate metabolism to myocardial metabolism and function.

Altered cardiac metabolism may contribute to the complex pathophysiology and inexorable progression of heart failure (HF)[1]. Metabolic flexibility enables the healthy heart to effectively utilize multiple substrates to sustain ATP generation based on substrate availability and hemodynamic conditions. Fatty acid oxidation (FAO) contributes about 70% of baseline myocardial energy requirements[2], with important contributions from glucose and lactate, which are crucial substrates for anaplerosis[3–5]. The heart also metabolizes amino acids and ketones, the importance of which might increase under certain pathologic conditions such as HF[4,6–11]. In response to stimuli that induce physiologic or pathologic cardiac hypertrophy, such as exercise training or pressure overload, respectively, glucose and lactate assume increased importance as energy sources[12,13]. The majority of glucose enters glycolysis after conversion by hexokinase to glucose 6-phosphate (G6P). A smaller fraction is converted by aldose reductase to sorbitol in the polyol pathway. Additional metabolic fates of G6P include the pentose phosphate pathway (PPP), the hexosamine biosynthesis pathway (HBP) and glycogen synthesis[14,15]. Pathologic cardiac remodelling is associated with increased glycolysis, which might not be matched by increased glucose oxidation[16–18]. This metabolic imbalance has been hypothesized to contribute to impaired myocardial contractility in pathologic cardiac hypertrophy and HF[17].

Pyruvate is the key metabolite connecting glycolysis and glucose oxidation. After entering the mitochondria, pyruvate undergoes decarboxylation (pyruvate decarboxylation (PDC); oxidation) to acetyl-CoA by the pyruvate dehydrogenase complex (PDH), which then enters the citric acid cycle (CAC). Pyruvate is also carboxylated, supporting CAC anaplerosis, by pyruvate carboxylation to oxaloacetate (OAA) via carboxylation by either pyruvate carboxylase (PC) or cytosolic malic enzyme 1 (ME1), which, in the heart, is more abundant than PC[5,19–22]. Decarboxylation is the dominant fate of pyruvate in mitochondria of healthy myocardium[23–25] and anaplerosis from pyruvate carboxylation represents 10% or less of total CAC flux[21,22].

[1]Fraternal Order of Eagles Diabetes Research Center, Carver College of Medicine, University of Iowa, Iowa City, IA, USA. [2]Division of Endocrinology and Metabolism, Carver College of Medicine, University of Iowa, Iowa City, IA, USA. [3]Department of Nutrition, Université de Montréal and Montreal Heart Institute, Montreal, Canada. [4]Sanford Burnham Prebys Medical Discovery Institute, Orlando, FL, USA. [5]Friedrich-Schiller University of Jena, Jena, Germany. [6]Mouse Metabolic Phenotyping Core, Carver College of Medicine, University of Iowa, Iowa City, IA, USA. [7]Metabolomics Core Facility, Carver College of Medicine, University of Iowa, Iowa City, IA, USA. [8]Division of Molecular Medicine, Department of Medicine, University of Minnesota, Minneapolis, MN, USA. [9]Abboud Cardiovascular Research Center, Carver College of Medicine, University of Iowa, Iowa City, IA, USA. [10]Department of Biochemistry, School of Medicine, University of Utah, Salt Lake City, UT, USA. [11]Metabolomics Core Research Facility, School of Medicine, University of Utah, Salt Lake City, UT, USA. [12]Howard Hughes Medical Institute, School of Medicine, University of Utah, Salt Lake City, UT, USA. [13]Department of Molecular Physiology and Biophysics, Carver College of Medicine, University of Iowa, Iowa City, IA, USA. [14]Department of Internal Medicine and Davis Heart and Lung Research Institute, The Ohio State University College of Medicine, Columbus, OH, USA. ✉e-mail: DRCAdmin@uiowa.edu

The discovery of the high-affinity MPC complex has advanced the understanding of mitochondrial pyruvate partitioning and its metabolic consequences[26–28]. The MPC is a mitochondrial inner-membrane protein complex composed of two subunits, MPC1 and MPC2. Both are essential for maintaining normal function of the MPC and loss of either subunit impairs mitochondrial pyruvate transport and pyruvate-supported oxygen consumption[26,28]. Embryonic deletion of the MPC is incompatible with embryonic survival[29]. MPC deficiency in mouse liver reduced pyruvate-driven gluconeogenesis and these animals resisted high-fat diet (HFD)-induced hyperglycaemia, insulin resistance and hepatic fibrosis[30–32]. Disruption of the MPC in skeletal muscle increased muscle glucose uptake and whole-body energy expenditure[33]. The contribution of mitochondrial pyruvate uptake and metabolism in normal and failing hearts is incompletely understood, although induction of MPC expression, in peri-infarct zones from patients with ischemic cardiomyopathy, has been proposed to represent an adaptive response that promotes cardioprotection[34].

The present study undertook detailed characterization of mice with cardiomyocyte-selective deletion of MPC1 under stressed and non-stressed conditions (cMPC1$^{-/-}$). Initial mitochondrial adaptations included MPC-independent pathways for acetyl-CoA generation from pyruvate via PDC but not for anaplerosis. Although associated with increased left ventricular (LV) contractility, increased relative contribution to CAC from pyruvate and preserved CAC intermediates, FAO was increased and acyl-carnitines, glycogen, pyruvate, lactate and O-linked *N*-acetylglucosamine (*O*-GlcNAc) modifications were accumulated. These initial adaptations paralleled pathologic LV hypertrophy and rapid progression to HF with pressure overload. They also developed an age-dependent dilated cardiomyopathy in concert with declining acetyl-CoA, citrate and ATP. Increasing the dietary supply of alternative metabolic substrates such as ketones, fatty acids or triglycerides prevented the accumulation of lactate and pyruvate and reversed pathologic remodelling. These data indicate an essential role for MPC-derived pyruvate for sustaining CAC function (oxidation and anaplerosis) in response to hemodynamic stress, and reveal potential cardiac toxicity of accumulated glycolytic intermediates.

Results

Generation of cMPC1$^{-/-}$ mice. MPC1 cardiomyocyte-specific knockout mice (cMPC1$^{-/-}$ mice) were generated by crossing MPC1-floxed mice with mice expressing Cre recombinase controlled by the alpha myosin heavy chain (*MYH6* or αMHC) promoter[30,35]. The cMPC1$^{-/-}$ mice were viable at birth and developed normally. MPC1 messenger RNA was decreased in whole-heart homogenates, whereas MPC2 mRNA remained unaltered (Fig. 1a). Western blot analysis in isolated cardiomyocytes revealed no detectable MPC1 and MPC2 protein in cMPC1$^{-/-}$ mice (Fig. 1b,c). Residual MPC protein in whole-heart homogenates probably reflects MPC expression in non-cardiomyocytes (Extended Data Fig. 1a,b). Pyruvate uptake in cMPC1$^{-/-}$ mitochondria was reduced by 75% relative to wild-type (WT) controls (Fig. 1d). Basal and maximal pyruvate-supported mitochondrial oxygen consumption was also reduced by 32% and 43%, respectively (Fig. 1e). Basal or maximal glutamate or palmitoyl-carnitine-supported respiration rates were not impaired (Fig. 1f and Extended Data Fig. 1c). Mitochondrial ultrastructure, electron transport chain subunit content and DNA copy number were unchanged in hearts of 4- or 8-week-old cMPC1$^{-/-}$ mice (Extended Data Fig. 1d–g).

The cMPC1$^{-/-}$ mice develop age-dependent cardiac hypertrophy and cardiac dysfunction. No significant difference was observed in cardiac structure, ejection fraction, LV chamber mass or heart weight normalized to tibia length (HW:TL) in cMPC1$^{-/-}$ at age 4 weeks (Fig. 1g–j). By age 8 weeks, cMPC1$^{-/-}$ mice developed concentric LV hypertrophy (LVH) with preserved ejection fraction (Fig. 1g–j). LV function progressively declined thereafter, as evidenced by LV dilatation and reduced ejection fraction, which was clearly evident in 18-week-old mice and inexorably progressed until death (Figs. 1g–j,l). Consistent with pathologic LVH, expression of the hypertrophic markers, ANP, BNP and acta1 (Fig. 1k), was dramatically induced at age 8 weeks.

Metabolic characterization of cMPC1$^{-/-}$ hearts. To further explore metabolic changes that could provide information on mechanisms underlying cardiac dysfunction in the absence of MPC, a detailed characterization of myocardial substrate metabolism was undertaken in hearts of 8-week-old cMPC1$^{-/-}$ mice at the stage of compensated pathologic LVH.

Substrate oxidation in isolated working hearts. Glucose oxidation was reduced by 50% but glycolysis was not altered in cMPC1$^{-/-}$ hearts (Fig. 2a,b). FAO was increased by ~55% in cMPC1$^{-/-}$ hearts, whereas the myocardial oxygen consumption rate (MVO_2) was decreased by ~28% (Fig. 2c,d). Cardiac power was increased by ~2.4-fold and cardiac efficiency was significantly increased by 8% in cMPC1$^{-/-}$ hearts (Fig. 2e,f).

Fate of glycolytic intermediates. Although glycolytic flux in isolated working hearts was not increased, glycolytic intermediates determined by gas chromatography/mass spectrometry (GC/MS) analysis were increased in cMPC1$^{-/-}$ hearts collected by freeze clamping in situ. G6P, G1P and pyruvate were increased by ~2.6-fold, ~1.8-fold and ~1.8-fold, respectively (Extended Data Fig. 2a). Protein levels of glycolysis enzymes (hexokinase I and glyceraldehyde 3-phosphate dehydrogenase) isolated from cardiomyocytes were increased by ~1.4-fold and ~1.3-fold, respectively, in cMPC1$^{-/-}$ hearts (Extended Data Fig. 2b). The intermediate of the PPP, sedoheptulose 7-phosphate (S7P), was also increased by ~2.1-fold (Extended Data Fig. 2a). *O*-GlcNAc protein modifications—a proxy of flux through the HBP—and glycogen content were determined in hearts from 8-week-old control and cMPC1$^{-/-}$ mice. The cMPC1$^{-/-}$ hearts exhibited a 76% increase in total *O*-GlcNAc protein modification (Fig. 2g,h) and a 70% increase in levels of the enzyme *O*-GlcNAc transferase (Extended Data Fig. 2b). Under both fed and overnight fasting (18 h fasting) conditions, glycogen storage was increased by ~4.2-fold and ~1.4-fold in cMPC1$^{-/-}$ hearts, respectively (Fig. 2i). In addition, total glycogen synthase protein and its phosphorylation level were increased in cMPC1$^{-/-}$ hearts (Extended Data Fig. 2b). These data indicate that glucose is shunted into alternative glucose metabolic pathways such as the PPP, the HBP and glycogen in cMPC1$^{-/-}$ hearts.

Metabolomics analysis in perfused cMPC1$^{-/-}$ hearts. To evaluate metabolite partitioning in cMPC1$^{-/-}$ hearts in greater detail, we perfused an independent cohort of hearts from 8-week-old control and cMPC1$^{-/-}$ mice with unlabelled substrates in the Langendorff mode and subjected to metabolomics analysis using GC/MS. Tissue levels of pyruvate, alanine and serine were increased in cMPC1$^{-/-}$ hearts, but lactate and ketone bodies (β-hydroxybutyrate (β-HB) and acetoacetate (AcAc)) concentrations were unchanged (Fig. 3a–f). The increase in pyruvate is consistent with restricted mitochondrial pyruvate entry, and increased alanine suggests increased conversion of accumulated pyruvate to alanine by alanine transaminase (ALT). Tissue concentrations of the CAC intermediates citrate, α-ketoglutarate (α-KG), succinate, fumarate and malate were not significantly changed in cMPC1$^{-/-}$ hearts (Fig. 3g). The ratios lactate:pyruvate and β-HB:AcAc reflect the ratio of NADH:NAD$^+$ in the cytosol and mitochondria, respectively[23,36]. In cMPC1$^{-/-}$ hearts, the lactate:pyruvate ratio was reduced but the β-HB:AcAc ratio was unchanged (Fig. 3h,i), which suggests that the

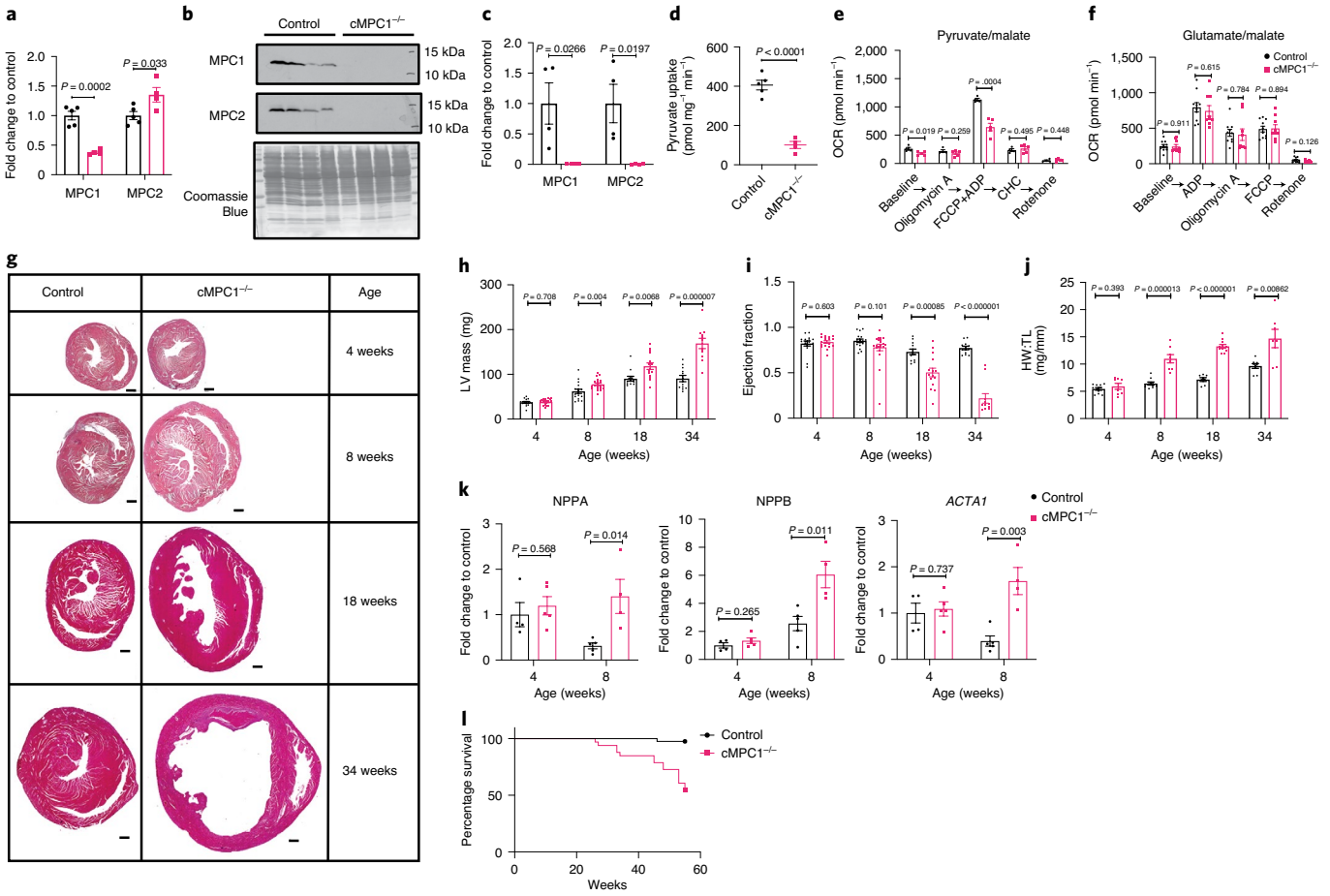

Fig. 1 | Generation and phenotype of cMPC1$^{-/-}$ mice. a–c, Loss of MPC1 was confirmed by qPCR (**a**) in heart lysates of 4-week-old cMPC1$^{-/-}$ mice (sample size, $n=5$, control; $n=4$, cMPC1$^{-/-}$) and western blots (**b**; quantification shown in **c**) in isolated cardiomyocytes from 8-week-old cMPC1$^{-/-}$ mice ($n=4$, control; $n=5$, cMPC1$^{-/-}$). **d**, Mitochondrial pyruvate uptake was performed in mitochondria isolated from 8-week-old cMPC1$^{-/-}$ hearts ($n=5$, control; $n=4$, cMPC1$^{-/-}$). **e**,**f**, Oxygen consumption rates (OCR) were determined by seahorse respirometry in isolated mitochondria from 8-week-old cMPC1$^{-/-}$ hearts in the presence of pyruvate (1 mmol l^{-1})/malate (0.25 mmol l^{-1}) (**e**) ($n=4$, control; $n=4$, cMPC1$^{-/-}$) and glutamate (1 mmol l^{-1})/malate (0.25 mmol l^{-1}) (**f**) ($n=10$, control; $n=9$, cMPC1$^{-/-}$). The concentration of the MPC inhibitor (CHC) was 1 mM. See Methods for concentrations of other inhibitors. **g**, Midventricular cross-sections of cMPC1 and control hearts at the ages shown. Scale bar, 500 µm. Images represent $n=3$ per group. **h**,**i**, LV mass (**h**) and ejection fraction (EF, **i**) by echocardiography. **j**, HW:TL at the ages shown (n is represented as control/cMPC1$^{-/-}$) (for **h** and **i**, age 4 and 8 weeks: 17/21; age 18 weeks: 12/15; age 34 weeks: 12/12; for **j**, age 4 weeks: 11/8; age 8 weeks: 10/8; age 18 weeks: 7/11; age 34 weeks: 8/7). **k**, The mRNA levels of hypertrophic genes, *ANP* (NPPA), *BNP* (NPPB) and *ACTA1* were determined by qPCR in 4- and 8-week-old cMPC1$^{-/-}$ hearts (age 4 weeks: 4/5; age 8 weeks: 5/4). **l**, Survival curves of control and cMPC1$^{-/-}$ mice over a 1-year period ($n=34$, control; $n=30$, cMPC1$^{-/-}$). Data are presented as mean ± s.e.m. and analysed using two-tailed, unpaired Student's *t*-tests.

redox state was maintained in mitochondria, but not in the cytosol. The lower lactate:pyruvate ratio reflects increased NAD$^+$ relative to NADH, which suggests that the cytoplasmic redox state became more oxidized in cMPC1$^{-/-}$ hearts.

Carbon isotopomer flux analysis in cMPC1$^{-/-}$ hearts. To further determine the metabolic fate of glucose-derived carbons, Langendorff perfusions were conducted using a modified Krebs buffer containing a mixture of substrates at physiologic concentrations including uniformly labelled [U-$^{13}C_6$]glucose (Extended Data Fig. 3). The ^{13}C-labelled molar percentage enrichment (MPE) of pyruvate, lactate and alanine, but not serine, was increased in cMPC1$^{-/-}$ mouse hearts (Fig. 4a and Extended Data Fig. 4a–d). The increased ^{13}C-labelled MPE of pyruvate and lactate supports accumulation of glycolytic intermediates and flux into pyruvate and lactate versus conversion from lactate to pyruvate via lactate dehydrogenase. Increased ^{13}C-labelled MPE of alanine is consistent with increased relative flux of accumulated pyruvate into alanine by ALT. No changes were observed in the MPE of M+2 pyruvate (Extended Data Fig. 4a), suggesting that the proportional contribution from the PPP to pyruvate was not increased relative to glycolytic flux. In addition, the MPE of M+3 serine was not significantly changed between control and cMPC1$^{-/-}$ hearts (Extended Data Fig. 4d), suggesting that the relative flux into the serine biosynthesis pathway (SBP) of glycolytic intermediates derived from exogenous glucose was not increased in cMPC1$^{-/-}$ hearts.

Although tissue concentrations of CAC intermediates were maintained in cMPC1$^{-/-}$ hearts, the ^{13}C-labelled MPE of these CAC intermediates was increased (Fig. 4b). PC flux (contributed by both PC and ME1) and PDC flux relative to citrate synthase (CS) were calculated from tissue ^{13}C-labelled MPE of isotopomers of citrate, pyruvate, the OAA moiety of citrate (OAA^{CIT}) and succinate[37]. Although PC:CS and PDC:CS flux ratios were not significantly changed in cMPC1$^{-/-}$ hearts (Fig. 4c,d), the flux ratio PC:PDC was significantly reduced in cMPC1$^{-/-}$ hearts (Fig. 4e), indicating that PDC flux is maintained or increased in cMPC1$^{-/-}$

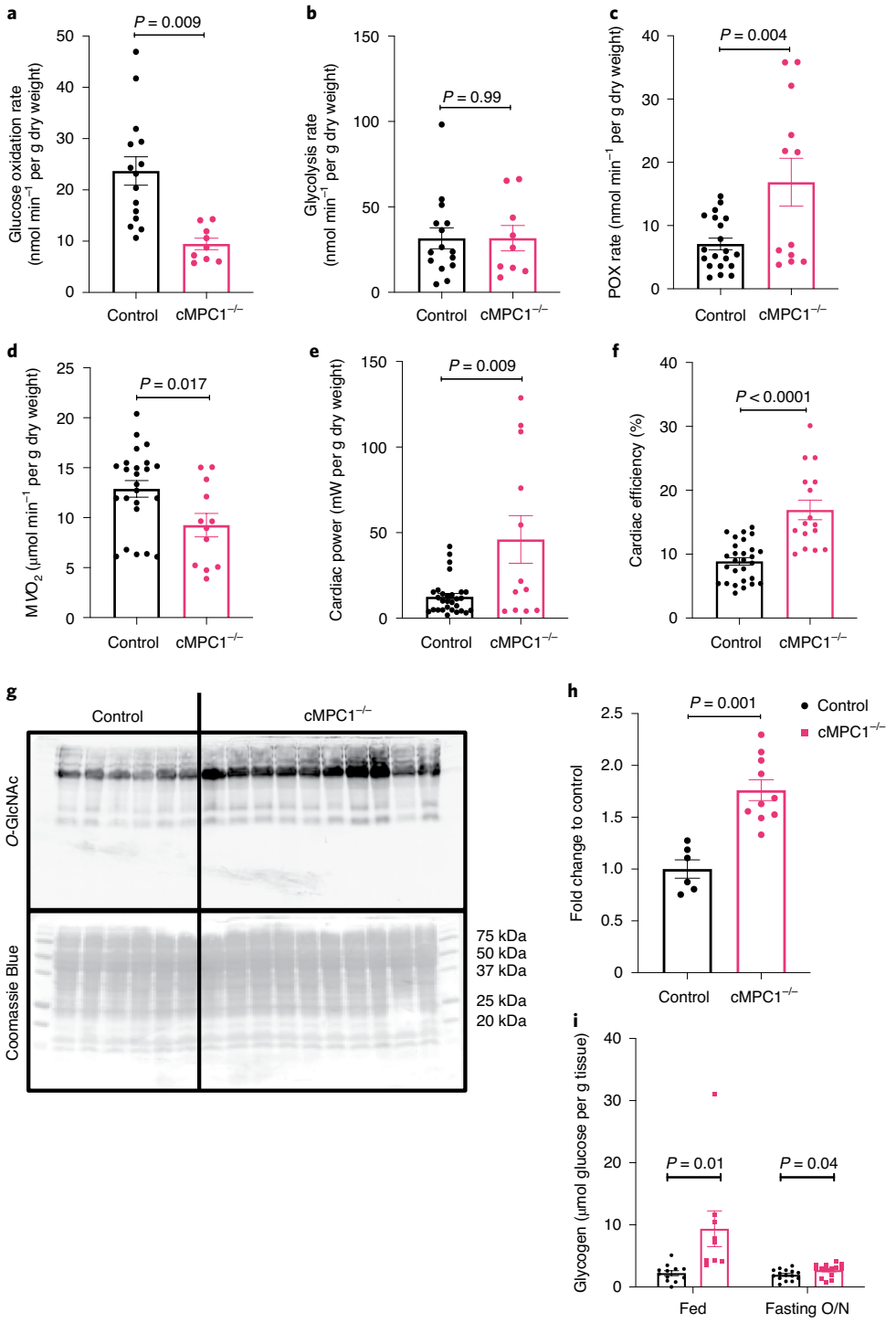

Fig. 2 | Substrate metabolism and partitioning in cMPC1$^{-/-}$ hearts. a–f, Hearts from 8-week-old control and cMPC1$^{-/-}$ mice were perfused with either [^{14}C]/[^{3}H]glucose (5 mM) or [^{3}H]palmitate (0.4 mM) with unlabelled pyruvate (0.5 mM) and lactate (1 mM), in the working heart mode to determine glucose oxidation (**a**), glycolysis (**b**) and FAO (**c**), respectively. MVO_2 (**d**), cardiac power (**e**) and cardiac efficiency (**f**) were also determined in the [^{3}H] palmitate-perfused hearts shown in **c**. Three replicates were obtained in each heart for **a–f** ($n = 7$, control; $n = 4$, cMPC1$^{-/-}$). HBP flux was estimated by quantification of *O*-GlcNAc modifications by western blotting (**g**; quantification shown in **h**) in hearts from 8-week-old control and cMPC1$^{-/-}$ mice (control, $n = 6$; cMPC1$^{-/-}$, $n = 10$). **i**, Glycogen content was measured in the hearts from 8-week-old control and cMPC1$^{-/-}$ mice under fed and overnight (O/N) fasting conditions (fed: control, $n = 12$; cMPC1$^{-/-}$, $n = 9$; fasting: control, $n = 15$; cMPC1$^{-/-}$, $n = 14$). Data are presented as mean ± s.e.m. and analysed using two-tailed, unpaired Student's *t*-tests.

hearts, without a concurrent increase in PC flux. Consistent with the reduced PC:PDC flux ratio, the percentage of recycled [^{13}C] citrate metabolized into the CAC (percentage citrate recycling, calculated from the tissue ^{13}C-labelled MPE of isotopomers of citrate, succinate and OAA^{CIT} (ref. [25])) was increased in cMPC1$^{-/-}$ hearts (Fig. 4f). These observations were independently validated

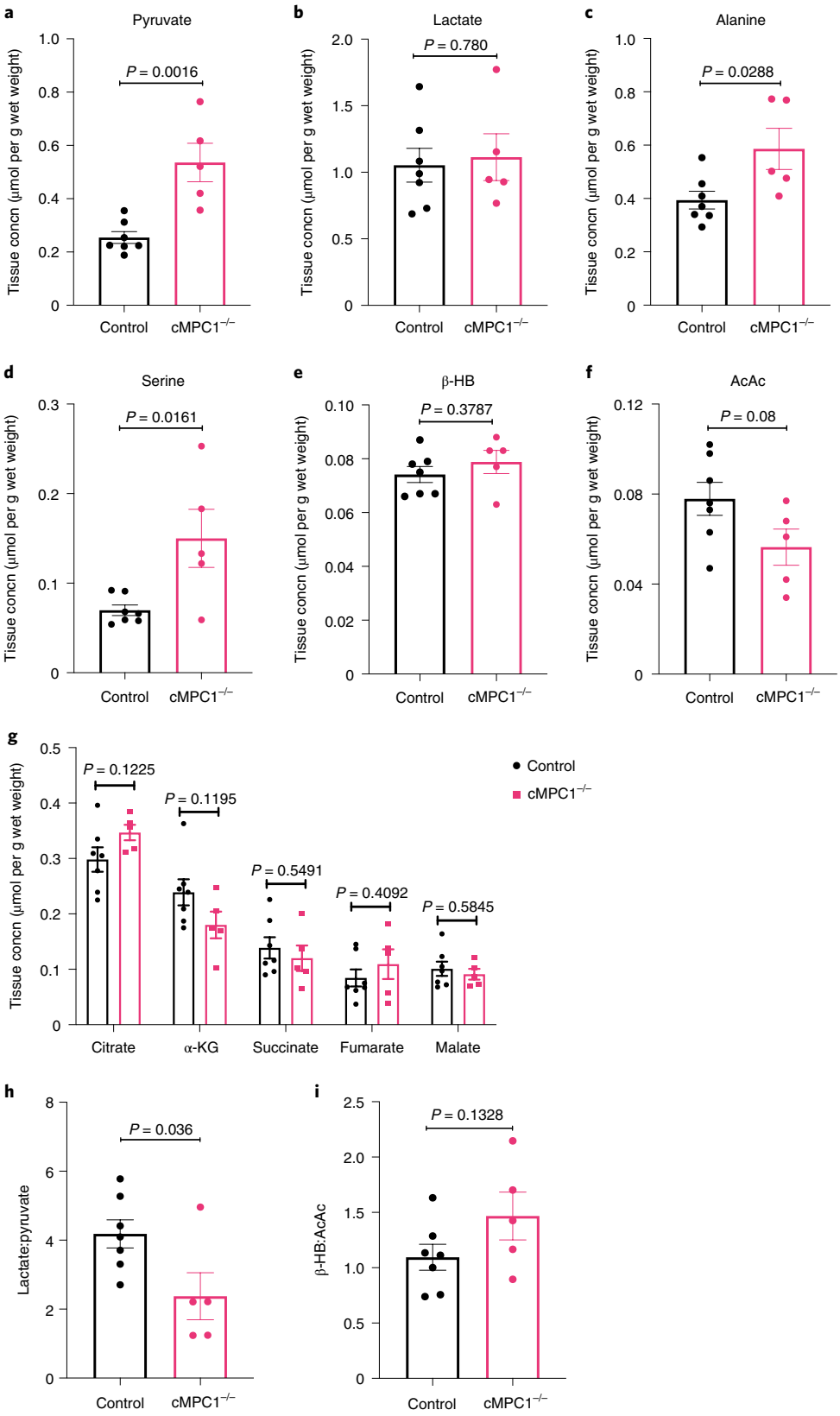

Fig. 3 | Concentrations of metabolic intermediates in perfused cMPC1$^{-/-}$ hearts. Metabolite concentrations determined in Langendorff-perfused, 8-week-old hearts perfused with unlabelled substrates (10 mM glucose, 0.4 mM palmitate, 0.5 mM lactate, 0.1 mM β-HB and 0.5 mM glutamine). **a**–**g**, Tissue concentrations of pyruvate (**a**), lactate (**b**), alanine (**c**), serine (**d**), ketones (**e**, β-HB; **f**, AcAc) and CAC intermediates (**g**) were determined by GC/MS (control, $n=7$; cMPC1$^{-/-}$, $n=5$). **h**,**i**, The ratios lactate:pyruvate (**h**) and β-HB:AcAc (**i**) were calculated using tissue concentrations of lactate (**b**), pyruvate (**a**), β-HB (**e**) and AcAc (**f**). Data are presented as mean ± s.e.m. and *P* values were determined using two-tailed, unpaired Student's *t*-tests.

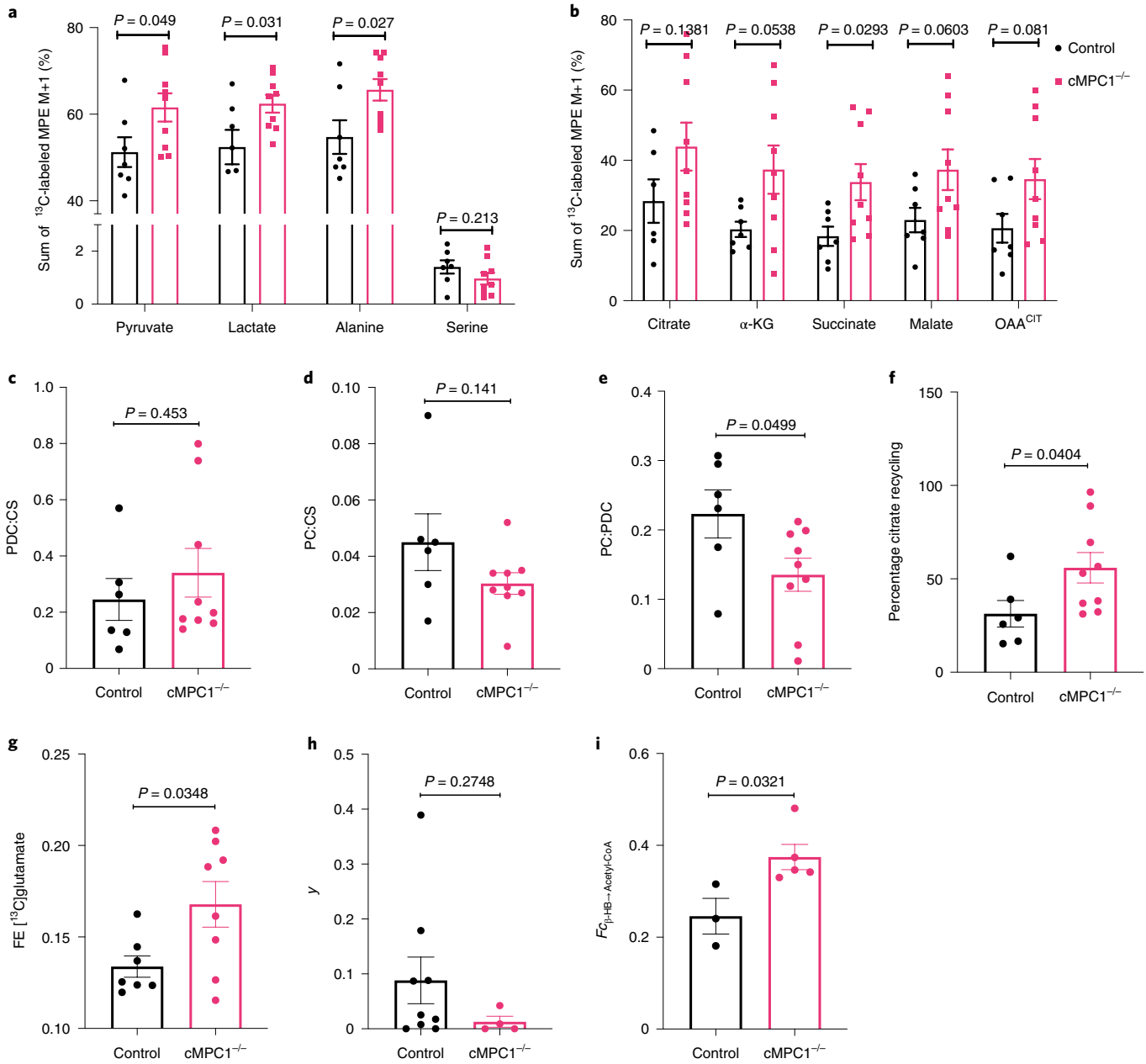

Fig. 4 | ^{13}C-labelled enrichment of metabolites in ^{13}C-labelled, substrate-perfused cMPC1$^{-/-}$ hearts. a–d, Metabolic flux analysis of Langendorff hearts from 8-week-old mice perfused with 10 mM [U-$^{13}C_6$]glucose and unlabelled substrates (0.4 mM palmitate, 0.5 mM lactate, 0.1 mM β-HB and 0.5 mM glutamine). Total MPE of all ^{13}C-labelled isotopomers of tissue pyruvate, lactate, alanine, serine (**a**) and CAC intermediates (**b**) were determined by GC/MS (control, $n=6$; cMPC1$^{-/-}$, $n=9$). **c–f**, The flux ratios of PDC:CS (**c**), PC:CS (**d**), PC:PDC (**e**) and percentage of [^{13}C]citrate recycling into CAC (**f**) were calculated from tissue ^{13}C-labelled MPE of isotopomers of citrate, the OAA^{CIT}, pyruvate and succinate (control, $n=6$; cMPC1$^{-/-}$, $n=9$). **g**, Fractional enrichment (FE) analysis of [^{13}C]glutamate performed on neutralized acid extracts of Langendorff hearts perfused with 10 mM [1,6-$^{13}C_2$]glucose, 0.5 mM [3-^{13}C]-pyruvate and 1 mM [3-^{13}C]lactate, in addition to 0.4 mM unlabelled palmitate (control, $n=7$; cMPC1$^{-/-}$, $n=8$). **h**, Ratio of anaplerosis to CS flux (y) was determined in neutralized acid extracts of Langendorff hearts perfused with 0.4 mM [U-^{13}C]palmitate, in addition to unlabelled substrates (10 mM glucose, 0.5 mM pyruvate and 1 mM lactate) (control, $n=9$; cMPC1$^{-/-}$, $n=4$). **i**, Langendorff perfusion was performed with 0.5 mM [2,4-$^{13}C_2$]β-HB and unlabelled substrates (10 mM glucose, 0.4 mM palmitate, 0.5 mM pyruvate and 1 mM lactate) (control, $n=3$; cMPC1$^{-/-}$, $n=5$). Neutralized acid extracts were analysed by NMR to determine fractional ^{13}C enrichment of acetyl-CoA entering the CAC from oxidation of [^{13}C]β-HB ($Fc_{\beta\text{-HB}\rightarrow\text{Acetyl-CoA}}$). Data are presented as mean ± s.e.m. and P values were determined using two-tailed, unpaired Student's t-tests.

by NMR analysis of Langendorff-perfused hearts supplemented with [1,6-$^{13}C_2$]glucose and [3-^{13}C]pyruvate/lactate, in addition to unlabelled palmitate. The fractional enrichment of [^{13}C]glutamate was increased in cMPC1$^{-/-}$ hearts (Fig. 4g). Anaplerosis contributed by unlabelled carbohydrate, determined as the ratio of anaplerosis to CS (y), was not increased (Fig. 4h) when analysed by nuclear magnetic resonance (NMR) in hearts perfused with [U-$^{13}C_{16}$]palmitate, in addition to unlabelled substrates. These results identify potential MPC-independent auxiliary pathways by which pyruvate-derived carbons enter the mitochondria to generate acetyl-CoA, and changes in CAC intermediate metabolism or flux that increases the contribution of carbohydrate-derived

acetyl-CoA carbons to the CAC, when the MPC content is reduced. Notably, increased anaplerotic flux does not account for the MPC-independent increase in the relative contribution of glucose-derived acetyl-CoA carbons to the CAC in cMPC1$^{-/-}$ hearts at the compensated hypertrophy stage.

Increased ^{13}C-labelled enrichment of acetyl-CoA (Fig. 4i) in hearts perfused with β-[2,4-$^{13}C_2$]HB revealed increased ketone oxidation in cMPC1$^{-/-}$ hearts. Liquid chromatography/MS (LC/MS) revealed increased ^{13}C labelling of isotopomers of CAC intermediates (Extended Data Fig. 5), consistent with elevated utilization of ketones.

A KD reverses structural and functional remodelling in non-stressed cMPC1$^{-/-}$ hearts. Given the evidence for increased ketone oxidation in cMPC1$^{-/-}$ hearts and published evidence that a KD rescued embryonic lethality in germline MPC-deficient mice[29], we tested the hypothesis that increasing the delivery of ketones to cMPC1$^{-/-}$ hearts could ameliorate cardiac dysfunction. The first experiments used a KD that significantly raised circulating concentrations of the ketone body β-hydroxybutyrate (β-HB) by tenfold (Fig. 5a) and fibroblast growth factor 21 (FGF21; Fig. 5b). Four protocols for KD feeding were used, with mice placed on the KD at varying ages, characterized by progressive degrees of cardiac dysfunction. In protocol 1, KD was initiated at the time of weaning (age 3 weeks). Cardiac hypertrophy, LV dysfunction and the induction of pathologic hypertrophy genes were completely prevented after 15 weeks of KD feeding (Fig. 5d–g). No fibrosis was observed in either control or cMPC1$^{-/-}$ hearts on either the control diet or the KD (Fig. 5c). Thus, a KD prevents cardiac dysfunction induced by loss of MPC. In protocol 2, 10-week-old cMPC1$^{-/-}$ mice with established cardiac hypertrophy were placed on the KD, which reversed LVH and hypertrophic gene induction after 8 weeks of feeding (Fig. 6a,b and Extended Data Fig. 6). Thus, a KD leads to regression of LVH in cMPC1$^{-/-}$ mice with compensated LVH. In protocol 3, 18-week-old cMPC1$^{-/-}$ mice with reduced ejection fraction were placed on a KD. The increased LV mass and decreased ejection fraction were reversed by KD feeding for 8 weeks (Fig. 6c,d). However, in protocol 4, the dilated cardiomyopathy in 24-week-old cMPC1$^{-/-}$ mice was only partially reversed by KD feeding (Fig. 6e,f). The earliest evidence for interfibrillar fibrosis was observed in cMPC1$^{-/-}$ hearts at age 22 weeks (Fig. 6g,h). Taken together, KD reversed HF in cMPC1$^{-/-}$ mice before the development of fibrosis.

To examine the durability of KD protection, another cohort of 10-week-old mice was started on a KD for 8 weeks and then 50% of the mice for each genotype were randomized to remain on the KD or switched back to normal chow (2920X). Cardiac hypertrophy and HF re-developed in cMPC1$^{-/-}$ mice when placed back on normal chow (Extended Data Fig. 7). These results clearly indicate that the protection from a KD is present only as long as mice are consuming a KD.

HFD or ketone ester diet reverses cardiac structural remodelling in non-stressed cMPC1$^{-/-}$ hearts. The KD is a low-carbohydrate and high-fat diet, which increases fatty acid and ketone availability to the heart. To test whether the protective effects derived specifically from fat or ketone bodies, a HFD or a ketone ester (KE) diet was used to determine the specific impact of these fuels on cardiac structure and function in cMPC1$^{-/-}$ mice. The KE diet increased circulating concentrations of β-HB twofold (Fig. 6i) and was employed in 10-week-old mice (similar to KD protocol 2). Although cardiac hypertrophy was attenuated (Fig. 6j,k), a KE diet did not completely normalize heart weights. However, LV function was preserved (Fig. 6l). The non-ketogenic HFD, which was matched for micronutrients with the normal chow diet (NCD), was initiated in 10-week-old cMPC1$^{-/-}$ mice to mirror protocol 2. The HFD fully rescued cardiac hypertrophy and HF in cMPC1$^{-/-}$ mice, relative to animals on an NCD (Fig. 6m,n).

Metabolic adaptations to KD in non-stressed cMPC1$^{-/-}$ hearts. To explore potential mechanisms for the KD rescue, freeze-clamped hearts from both control and cMPC1$^{-/-}$ mice fed the control diet (2920X) or the KD were subjected to metabolomics analysis. Data from both GC/MS and LC/MS were combined and depicted on a heatmap (Fig. 7a). The principal component analysis (PCA) plot revealed distinct metabolomics profiles between control and cMPC1$^{-/-}$ hearts in mice fed the 2920X chow. However, the metabolomics pattern became overlapping in control and cMPC1$^{-/-}$ mice when fed the KD (Fig. 7b). The majority of acyl-carnitines, with chain lengths from 3:0 to 20:4, were increased in cMPC1$^{-/-}$ hearts relative to controls when fed 2920X chow (Fig. 7c). Moreover, on the KD, control hearts displayed increased acyl-carnitine accumulation. In contrast, cMPC1$^{-/-}$ hearts did not further increase acyl-carnitines on the KD, but maintained levels that were equivalent to those of controls on the KD (Fig. 7c). Accumulation of pyruvate and lactate in cMPC1$^{-/-}$ hearts was reversed by KD feeding (Fig. 7d). KD feeding also reduced the relative tissue concentration of glucose, G6P and fructose 6-phosphate. Together these data suggest that glucose uptake and glycolysis were markedly repressed in both control and cMPC1$^{-/-}$ hearts on a KD (Fig. 7d). A reduction in some CAC intermediates (acetyl-CoA and citrate; Fig. 7e) and ATP (Fig. 7f) was observed in the 14-week-old cMPC1$^{-/-}$ hearts compared with control hearts on 2920X chow, and these deficiencies were rescued by KD feeding (Fig. 7e,f). Accumulation of the PPP intermediate (S7P) and the SBP intermediates (serine and glycine) was reversed in the cMPC1$^{-/-}$ hearts fed with a KD (Fig. 7g). Some of the nucleotides, which were increased in cMPC1$^{-/-}$ hearts on 2920X chow, were normalized in cMPC1$^{-/-}$ hearts fed with a KD (Fig. 7h). Moreover, the increased glycogen storage and elevated protein *O*-GlcNAc modification in cMPC1$^{-/-}$ hearts were reversed by KD feeding (Fig. 7i–k). In conclusion, KD feeding reversed the accumulation of pyruvate and lactate, the decline in citrate and the shunting of glucose into alternative pathways (PPP, SBP, HBP and glycogen storage) in cMPC1$^{-/-}$ hearts that correlate with reversal of the age-dependent structural remodelling.

Divergent effects of short-term versus long-term KDs on cMPC1$^{-/-}$ mice after pressure overload. Given the striking effects of a KD in preventing or reversing LV remodelling in non-stressed cMPC1$^{-/-}$ hearts, we sought to determine whether this would modify the response of these hearts to hemodynamic stress. The cMPC1$^{-/-}$ mice were subjected to transverse aortic constriction (TAC) surgery. Young (6-week-old) control mice tolerate TAC and do not develop HF. However, 6-week-old cMPC1$^{-/-}$ mice exhibited accelerated LV remodelling and HF characterized by increased cardiac hypertrophy and fibrosis, and a greater reduction in the ejection fraction (Fig. 8a–e). To explore whether short-term KD feeding could ameliorate the exacerbated HF phenotype of cMPC1$^{-/-}$ mice under pressure overload (PO), 8-week-old mice were placed on a KD that was started at the time of TAC or maintained on a control diet (2920X). The cMPC1$^{-/-}$ mice on the control diet all died within 6 d of TAC surgery, whereas the mortality rate for WT mice was 20%. In the KD cohort, survival of WT mice was 100% within 1 week. However, all cMPC1$^{-/-}$ mice on the KD died within 5 d of TAC (Fig. 8f). Given that short-term KD feeding did not rescue the HF induced by TAC in cMPC1$^{-/-}$ mice, a separate cohort of mice fed with a KD, starting at weaning (age 3 weeks), was subjected to TAC surgery at the age of 6 weeks to explore the effect of long-term KD feeding. Then, 3 weeks after the TAC, the cMPC1$^{-/-}$ mice exhibited similar cardiac hypertrophy to control mice after TAC, and the ejection fraction was not decreased (Fig. 8g–i). Thus, long-term KD feeding prevented HF in cMPC1$^{-/-}$ mice without attenuating the hypertrophic response. To further characterize the impact of KD in WT mice, we compared the response to TAC in chow- and KD-fed WT mice. Cardiac hypertrophy attenuation was detected in young

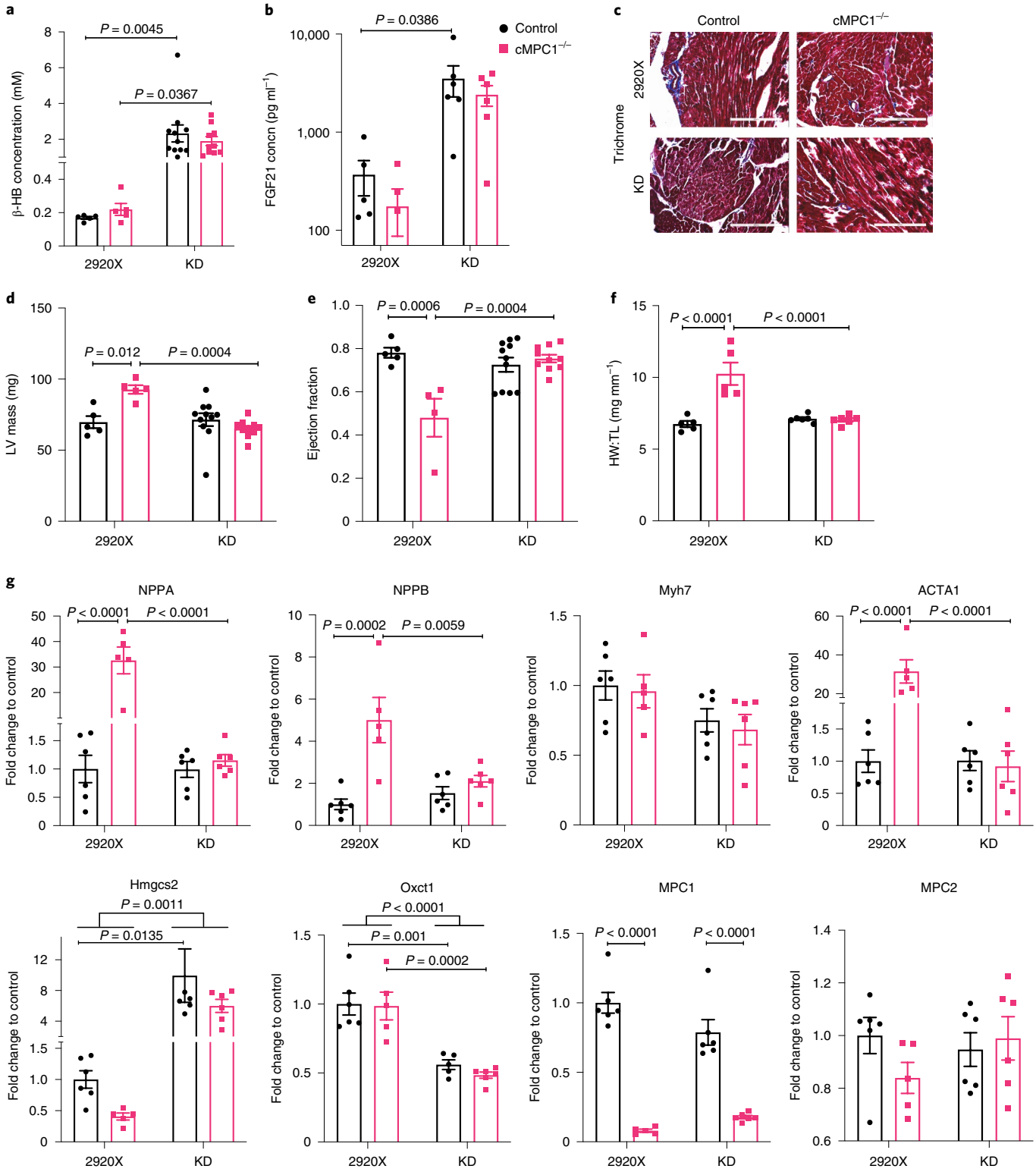

Fig. 5 | KD feeding prevents cardiac dysfunction in cMPC1$^{-/-}$ mice. Control and cMPC1$^{-/-}$ mice were fed with normal chow (2920X) or a KD at age 3 weeks. **a**,**b**, Serum concentration of β-HB (**a**) and FGF21 (**b**) after 8 weeks of feeding. **c**, Trichrome staining revealed no increase in cardiac fibrosis in cMPC1$^{-/-}$ mouse hearts. Scale bar, 200 μm. Images represent $n = 3$ per group. **d**,**e**, LV mass (**d**) and ejection fraction (**e**) were determined by echocardiography after 15 weeks of feeding. **f**,**g**, HW:TL (**f**) and gene expression analysis (**g**) were determined at the time of sacrifice after 18 weeks of feeding. For **a** and **d**–**f**, $n = 5$ (control-2920X), $n = 5$ (cMPC1$^{-/-}$-2920X), $n = 11$ (control-keto), $n = 10$ (cMPC1$^{-/-}$-keto); for **b**, $n = 5$ (control-2920X), $n = 5$ (cMPC1$^{-/-}$-2920X), $n = 6$ (control-keto), $n = 6$ (cMPC1$^{-/-}$-keto); for **g**, $n = 6$ (control-2920X), $n = 5$ (cMPC1$^{-/-}$-2920X), $n = 6$ (control-keto) and $n = 6$ (cMPC1$^{-/-}$-keto). Data are presented as mean ± s.e.m. and the P values were determined using two-way ANOVA followed by Tukey's multiple comparison test.

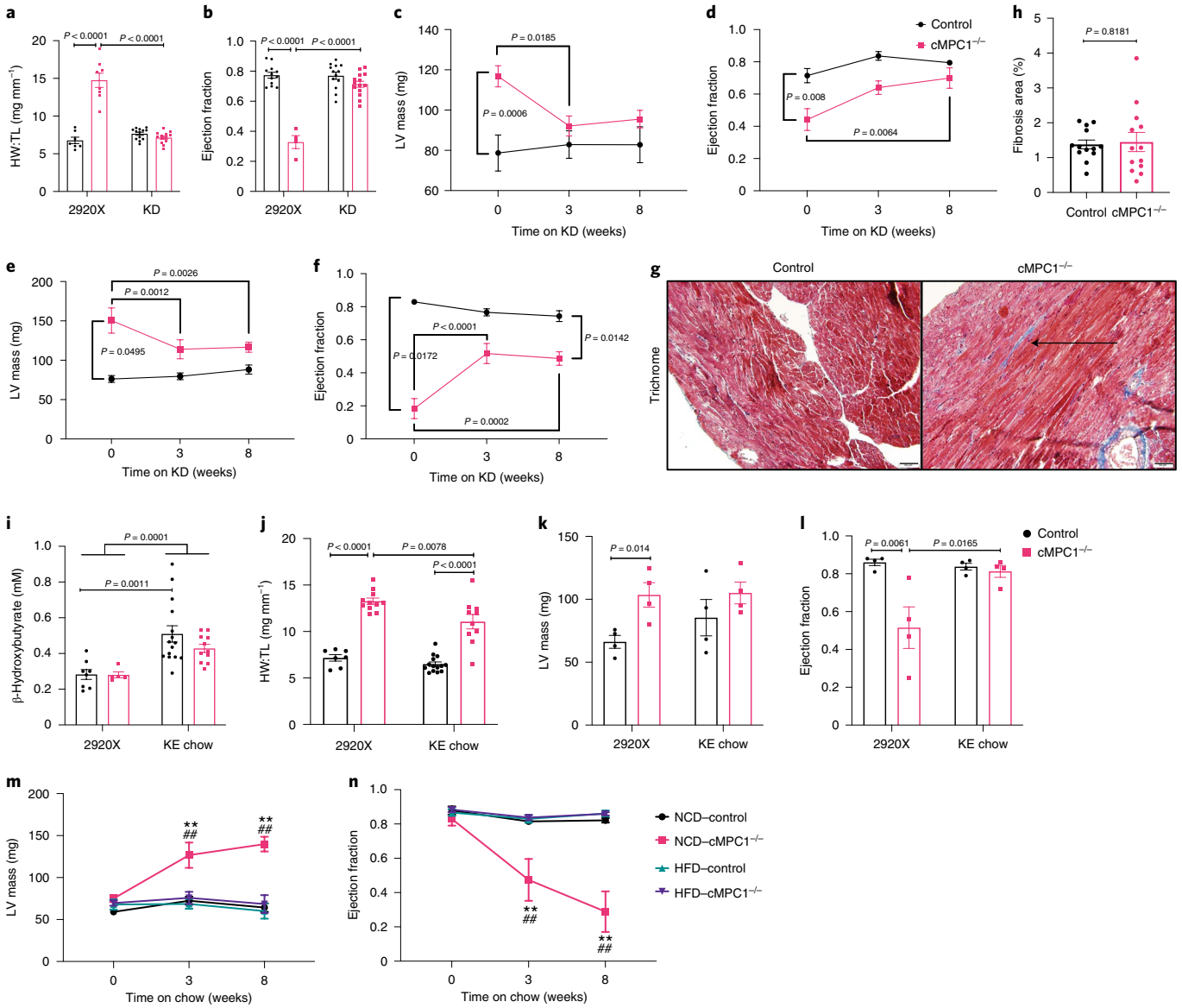

Fig. 6 | Alternative substrate feeding reverses cardiac dysfunction in cMPC1$^{-/-}$ mice. a–f, Three different cohorts of mice were fed with a KD at age 10 (**a**, **b**), 18 (**c**, **d**) and 24 (**e**, **f**) weeks. **a**,**b**, HW:TL (**a**) and ejection fraction (**b**) were determined after 8 weeks of a KD in the 10-week-old cohort. **c**–**f**, LV mass (**c**, **e**) and ejection fraction (**d**, **f**) were measured by echocardiography after 8 weeks in the 18- and 24-week-old cohorts, respectively. **g**,**h**, Trichrome-stained sections (**g**, quantification shown in **h**) revealed mild cardiac interfibrillar fibrosis in the 24-week-old cMPC1$^{-/-}$ mice. Scale bar, 50 µm. Images represent $n = 7$ (control)/$n = 6$ (cMPC1$^{-/-}$). For **a** and **b**, $n = 7$ (control-2920X), $n = 8$ (control-keto), $n = 13$ (cMPC1$^{-/-}$-2920X) and $n = 14$ (cMPC1$^{-/-}$-keto); for **c**–**f** and **h**: control-cMPC1$^{-/-}$, $n = 7/4$ (**c**, **d**), $n = 10/3$ (**e**, **f**) and $n = 7/6$ (**h**). **i**, Control and cMPC1$^{-/-}$ mice were fed with KE chow at age 10 weeks and the serum concentration of β-HB was determined after 2 weeks of feeding. **j**–**l**, HW:TL (**j**), LV mass (**k**) and ejection fraction (**l**) were determined after 8 weeks of KE chow feeding. **m**,**n**, Another cohort of mice was fed an NCD or a 60% HFD at age 10 weeks, and LV mass (**m**) and ejection fraction (**n**) were measured after 8 weeks of feeding by echocardiography. For **i** and **j**, $n = 8$ (control-2920X), $n = 5$ (cMPC1$^{-/-}$-2920X), $n = 15$ (control-KE) and $n = 11$ (cMPC1$^{-/-}$-KE); for **k** and **l**, $n = 4$ (all groups); for **m** and **n**, $n = 6$ (control-NCD), $n = 4$ (control-HFD), $n = 4$ (cMPC1$^{-/-}$-NCD) and $n = 5$ (cMPC1$^{-/-}$-HFD). Data are presented as mean ± s.e.m. and the *P* values were determined by a two-way ANOVA followed by Tukey's multiple comparison test. Control versus cMPC1$^{-/-}$: $^{**}P < 0.01$. Treatment versus baseline: $^{\#\#}P < 0.01$.

WT mice (age 6 weeks) after TAC surgery (Extended Data Fig. 8a–c) but not in 10-week-old WT mice (Extended Data Fig. 8d–f).

Discussion

The present study, demonstrating that loss of MPC in cardiomyocytes leads to age-dependent cardiac dysfunction and impaired substrate metabolism, provides interesting insights into the physiologic role of normal levels of MPC-dependent mitochondrial pyruvate uptake in the heart. First, we identified metabolic adaptations that develop in the heart, including the existence of potential alternative pathways for pyruvate mitochondrial entry, independent of anaplerosis, that are insufficient to maintain normal CAC activity in response to aging and hemodynamic stress. Second, we identified the existence of adaptive changes in fatty acid metabolism, which not only increase rates of FAO but also lead to accumulation of acyl-carnitines. Despite the existence of these adaptive mechanisms by which glucose-derived carbons could enter the CAC and an increased dependence on fatty acid metabolism, cMPC1$^{-/-}$ hearts

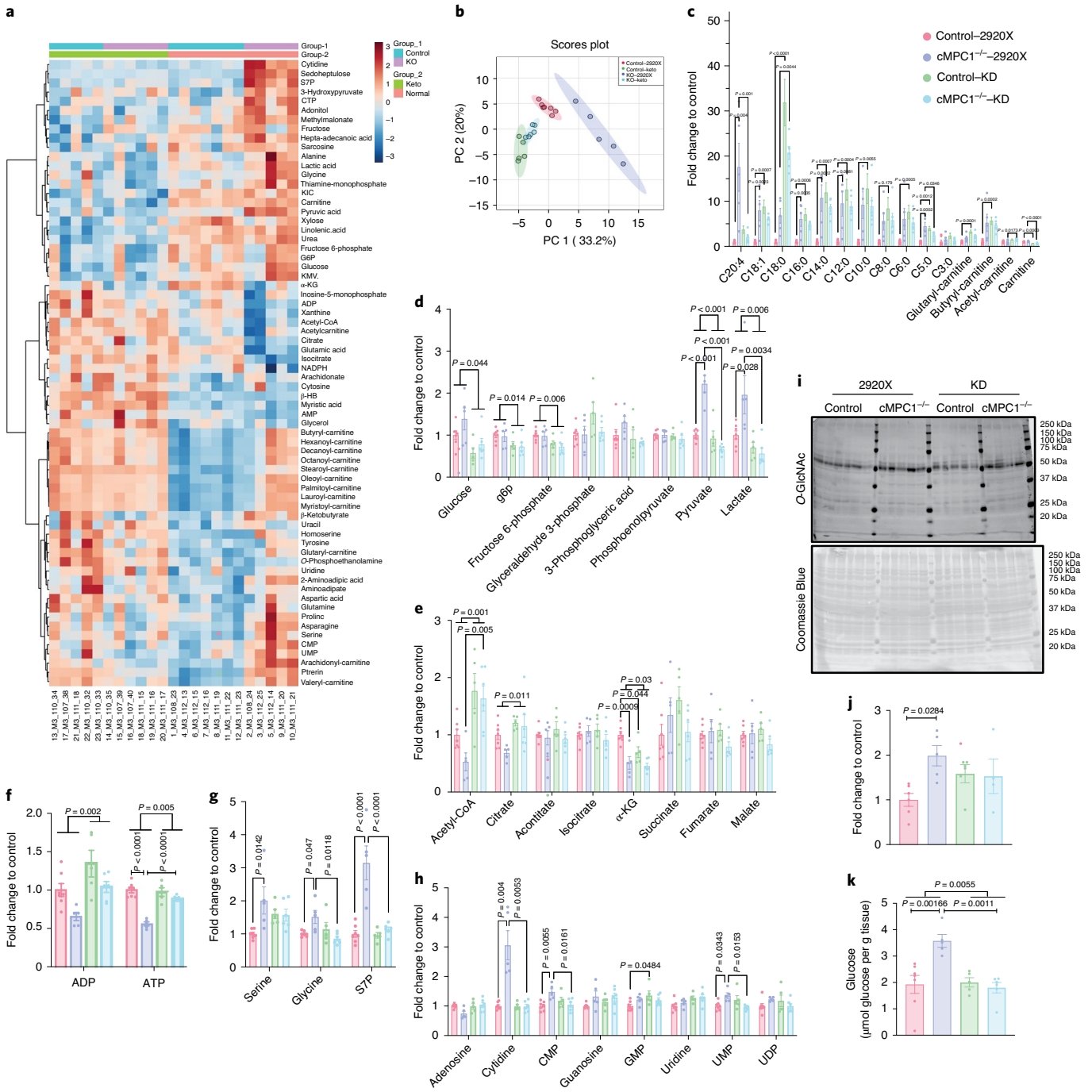

Fig. 7 | Metabolite profiles in KD hearts. Control and cMPC1$^{-/-}$ mice were fed with a KD starting at age 8 weeks and the hearts were freeze-clamped after 6 weeks of feeding. GC/MS and LC/MS were used to determine the levels of metabolites in the heart tissue. The fold change of all metabolites was normalized to control hearts fed on normal chow (2920X). **a**,**b**, A two-way heatmap (**a**) and PCA (**b**) were analysed and plotted by MetaboAnalyst. CTP, cytidine triphosphate; KIC, α-ketoisocaproate. **c**–**h**, Acyl-carnitines (**c**), glycolysis intermediates (**d**), CAC intermediates (**e**), ADP and ATP (**f**), PPP and SBP intermediates (**g**), and nucleotides (**h**) were plotted and analysed using a two-way ANOVA followed by Tukey's multiple comparison test. Sample sizes are as follows: $n=7$ (control–2920X), $n=5$ (cMPC1$^{-/-}$–2920X), $n=5$ (control-keto), $n=6$ (cMPC1$^{-/-}$-keto). **i**–**k**, *O*-GlcNAc blot (**i**) normalized to total Coomassie Blue staining (**j**) and glycogen storage (**k**) was determined in 18-week-old control and cMPC1$^{-/-}$ mice after 8 weeks of a KD (protocol 2). For **j**, sample sizes are as follows: $n=6$ (control–2920X), $n=5$ (cMPC1$^{-/-}$–2920X), $n=5$ (control-keto), $n=4$ (cMPC1$^{-/-}$-keto). For **k**, sample sizes are as follows: $n=7$ (control–2920X), $n=5$ (cMPC1$^{-/-}$–2920X), $n=5$ (control-keto), $n=6$ (cMPC1$^{-/-}$-keto). Data are presented as mean ± s.e.m. and analysed using a two-way ANOVA followed by Tukey's multiple comparison test. All *P* values <0.05 are shown on the figures. If not indicated, then *P* values are >0.05.

inexorably progress to failure. Reduced mitochondrial pyruvate uptake led to the accumulation of pyruvate and lactate in vivo and accumulation of pyruvate in perfused hearts, which recapitulate findings reported with chemical inhibitors of the MPC[38]. In addition, there was increased partitioning of glycolysis-derived metabolites into other cytosolic pathways such as glycogen synthesis, the

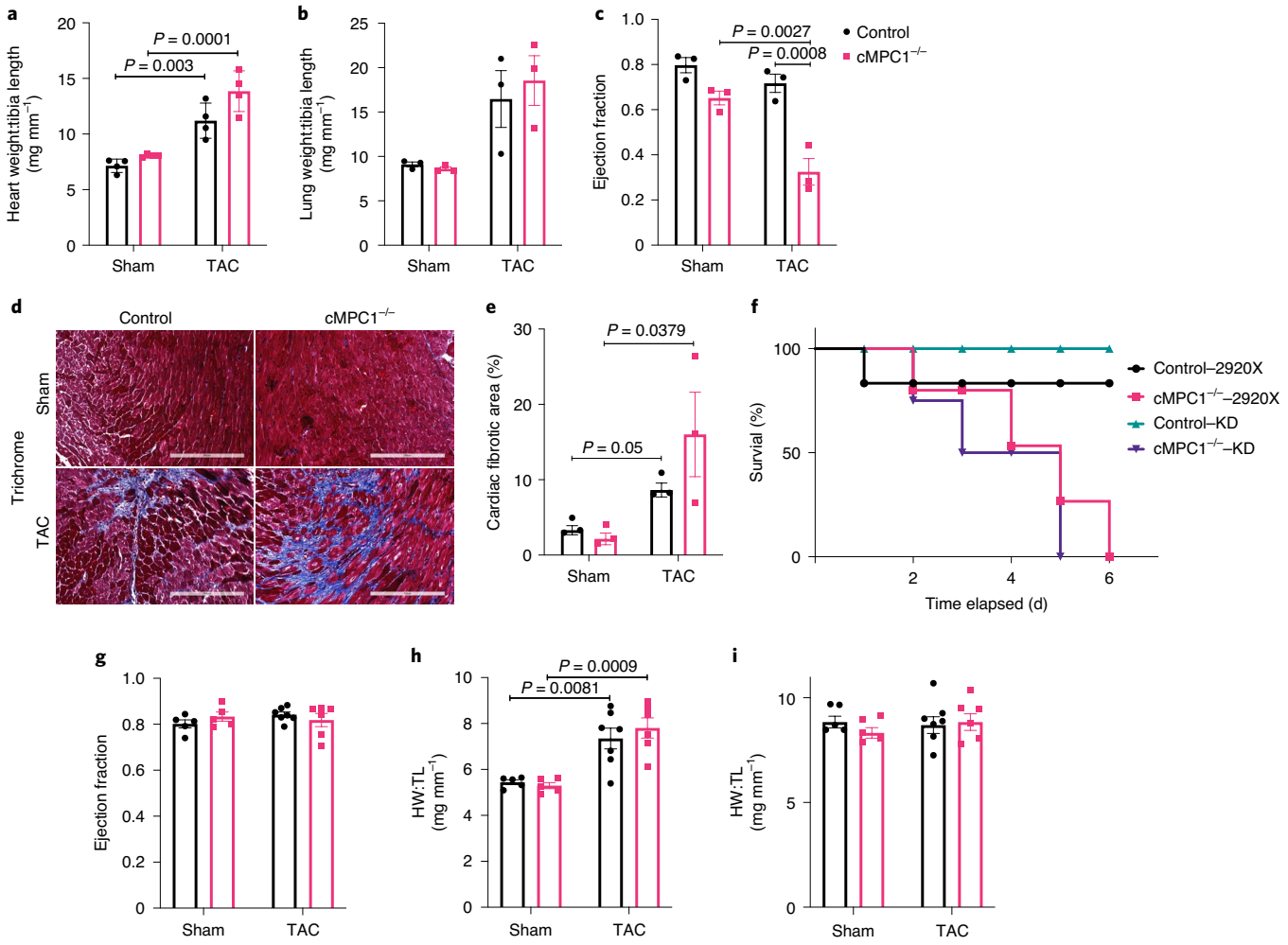

Fig. 8 | Divergent effects of KD feeding on PO-induced cardiac remodelling in cMPC1$^{-/-}$ mice. a–c, Control and cMPC1$^{-/-}$ mice were subjected to TAC surgery at the age of 6 weeks, and heart weights normalized to tibia length (**a**), lung weights normalized to tibia length (**b**) and ejection fraction (**c**) were determined 3 weeks after TAC. **d**,**e**, Cardiac fibrosis was revealed by trichrome staining (**d**) at the time of sacrifice and quantified (**e**). Scale bar, 200 µm. Images represent $n = 3$ per group. TAC surgery was performed on 8-week-old control and cMPC1$^{-/-}$ mice that were maintained on a chow diet or initiated on a KD at the time of TAC surgery. **f**, The survival curve after TAC. Control and cMPC1$^{-/-}$ mice were fed with a KD at weaning and were subjected to TAC surgery at age 6 weeks. **g–i**, Ejection fraction (**g**), heart weights normalized to tibia length (**h**) and lung weights normalized to tibia length (**i**) were assessed at 3 weeks after TAC. For **a–c** and **e**, $n = 3$ (all groups); for **f**, $n = 6$ (control-2920X), $n = 6$ (control-keto), $n = 7$ (cMPC1$^{-/-}$-2920X) and $n = 8$ (cMPC1$^{-/-}$-keto); for **g–i**, $n = 5$ (control-2920X), $n = 5$ (cMPC1$^{-/-}$-2920X), $n = 7$ (control-keto) and $n = 6$ (cMPC1$^{-/-}$-keto). Data are presented as mean ± s.e.m. and *P* values were determined using a two-way ANOVA followed by Tukey's multiple comparison test.

HBP, the PPP and the SBP, which in concert with changes in mitochondrial substrate utilization probably contributed to cardiac dysfunction. All of these metabolic abnormalities were reversed when animals were presented with supraphysiologic availability of alternative substrates such as ketones and fatty acids, which also prevented structural remodelling.

Determination of pyruvate uptake and respiration in isolated mitochondria in vitro revealed residual potential MPC-like pyruvate uptake activity in MPC1-deficient mitochondria. This could reflect supraphysiologic concentrations of pyruvate, used in in vitro assays, that could potentially lead to limited mitochondrial uptake via non-specific mechanisms such as carboxylate carriers with low affinity for pyruvate[39], or from MPC in non-cardiomyocyte mitochondria (Extended Data Fig. 1a). However, despite reduced mitochondrial pyruvate uptake, isotopomer analysis of [U-$^{13}C_6$] glucose-perfused hearts and fractional enrichment of [^{13}C]glutamate, from [1,6-$^{13}C_2$]glucose- and [3-^{13}C]pyruvate/lactate-perfused hearts at the stage of compensated cardiac hypertrophy, revealed the existence of robust adaptations by which pyruvate-derived carbons were entering the CAC acetyl-CoA pool, potentially via MPC-independent mechanisms such as malic enzyme or alanine transaminase, as previouslsy described in other tissues.

Cytosolic pyruvate can be converted to malate and alanine by ME1 and ALT1, respectively[40,41], both of which then enter mitochondria via specific shuttles. ME1 catalyses the conversion of cytosolic pyruvate to malate, accompanied by NADPH consumption[5,41,42]. ME1 has been reported to be an important source for anaplerosis and its expression level is significantly induced in rodent models of PO-induced pathologic hypertrophy[5]. In this context, cytosolic malate serves directly as an anaplerotic substrate via exchange with α-KG. However, carbon from this cytosolic malate need not enter the CAC cycle solely through anaplerosis, because the mitochondrial isoforms of malic enzyme, ME2 and ME3, could reconvert malate into pyruvate within the mitochondria for oxidation via PDH. Indeed, in the absence of elevated anaplerosis, and even at baseline levels of ME1 in the normal heart, the pathway

converting cytosolic pyruvate into malate, which enters the mitochondria, remains a source of mitochondrial pyruvate, via the action of ME2 and ME3. The ME redox pair (malate/pyruvate) was decreased in cMPC1$^{-/-}$ hearts, suggesting that the accumulated pyruvate could potentially drive the ME1 reaction to generate malate. However, tissue pyruvate was predominantly labelled in the M+3. This pattern does not support this mechanism because, if the transfer was occurring through malate, pyruvate should also be labelled at M+2 and M+1. M+3 labelling of pyruvate could predominate if there was no isotopic label randomization at fumarase, which is believed to be rapid, and if there was no mixing of labelled malate coming from ME, with that derived from the recycling of labelled citrate in the CAC. Although unlikely, this possibility cannot be ruled out.

Alanine and α-KG can be converted to pyruvate and glutamate, respectively, in mitochondria by the enzyme ALT2, which is highly expressed in heart[40]. The ^{13}C enrichment and absolute concentration of alanine were increased in cMPC1$^{-/-}$ hearts, raising the possibility that glucose- and pyruvate-derived carbons could enter the CAC in an MPC-independent manner via alanine, as was recently described in MPC-deficient livers[31]. However, tissue levels of α-KG were repressed. Moreover, the expression level of the cytosolic ALT isoform ALT1 is low in hearts[40] and the total ALT activity in cMPC1$^{-/-}$ hearts was not increased (Extended Data Fig. 9b,c). Although these data suggest that bypass via ALT might not represent the mechanism that increases pyruvate contribution to CAC acetyl-CoA in cMPC1$^{-/-}$ hearts at the compensated cardiac hypertrophy stage, specific experiments to support this conclusion, such as reducing ALT activity or expression or perfusing hearts with [2-^{13}C,U-$^{2}H_3$]pyruvate[43] to test for the role of alanine, were not performed. As such this mechanism cannot be completely ruled out.

Increased flux via the SBP could represent an alternative pathway for pyruvate carbons to enter the CAC in an MPC-independent manner. Although the total serine pool determined by metabolomics in in cMPC1$^{-/-}$ hearts was increased, the M+3 enrichment of serine was <1%. Thus, although the SBP was activated in cMPC1$^{-/-}$ hearts, there is no evidence from the labelling pattern of serine that the exogenous labelled glucose was contributing increased CAC labelling of intermediates via serine. An additional mechanism that was not directly tested in the present study is the possibility of increased mitochondrial lactate uptake and an intramitochondrial lactate–pyruvate shuttle, as recently proposed[44–46].

The metabolic impact of MPC deficiency in the heart differs profoundly from all other tissues in which this has previously been examined. Specifically, the metabolic reprogramming in cMPC1$^{-/-}$ hearts does not result in increased use of glutamine carbons for CAC metabolism (oxidative glutaminolysis) (Extended Data Fig. 10). This contrasts with other tissues such as liver, wherein the increased use of glutamine carbons for CAC metabolism was associated with higher pyruvate–alanine, among other pathways[30,31].

Although the specific mechanisms by which pyruvate enters the CAC when MPC levels or activity is reduced remains to be definitively elucidated, our metabolic analyses indicate that these adaptations appear to initially increase both cardiac efficiency and cardiac contractility in the short term, even when molecular evidence of pathologic LVH is present. However, decreased CAC intermediates and ATP in 14-week-old cMPC1$^{-/-}$ hearts (Fig. 7e,f) indicates that alternative routes or mechanisms for mitochondrial pyruvate utilization in the heart are insufficient in the long term to sustain LV function as these mice age. The possibility of CAC impairment is also supported by the observation that pyruvate flux to anaplerosis was not increased in cMPC1$^{-/-}$ hearts. Without MPC-dependent anaplerosis, the CAC pool could be sustained by increasing the recycling of CAC intermediates (Fig. 4f) in the short term, but this compensation mechanism is insufficient during aging or in the face of an acute hemodynamic load. Together, these data suggest a specific requirement for MPC in channelling or maintaining pyruvate availability for anaplerotic pathways.

Loss of mitochondrial pyruvate uptake in cardiomyocytes increased the accumulation of glycolytic intermediates, resulting in shunting of glucose into alternative pathways, such as SBP, PPP, HBP and glycogen storage. In [U-$^{13}C_6$]glucose-perfused cMPC1$^{-/-}$ hearts, the relative enrichment of M+2 pyruvate and M+3 serine was unchanged (Extended Data Fig. 4). However, total tissue levels of pyruvate and serine were increased in the perfused cMPC1$^{-/-}$ hearts (Fig. 3a,d), indicating that absolute abundance of M+2 pyruvate and M+3 serine was increased. These data suggest increased PPP and SBP flux in ex vivo perfused cMPC1$^{-/-}$ hearts. Moreover, metabolomics analysis from in situ (non-perfused) hearts revealed accumulation of the PPP intermediate S7P and the SBP intermediates serine and glycine in cMPC1$^{-/-}$ hearts (Extended Data Fig. 2a and Fig. 7g), consistent with increased shunting of glycolytic intermediates into the PPP and SBP in vivo. Metabolomics analysis also revealed increased nucleotide synthesis, suggesting that increased PPP flux may be supporting increased nucleotide synthesis (Fig. 7h). Increased glycogen (Fig. 2i) and *O*-GlcNAc content (Fig. 2g,h) in cMPC1$^{-/-}$ hearts indicates increased diversion of glucose into the HBP and glycogen synthesis, changes in which have been reported to correlate with pathologic cardiac remodelling[47,48].

The multiple metabolic and mitochondrial adaptations that develop in cMPC1$^{-/-}$ hearts inform potential mechanisms that may initially maintain cardiac function, but also contribute to the ultimate decline in cardiac function on an NCD versus the beneficial effect of KD. Although the auxiliary pathways by which pyruvate-derived carbons may enter the CAC to support CAC function in cMPC1$^{-/-}$ hearts in the short term, they are insufficient, as evidenced by accumulation of lactate and pyruvate, and increased diversion of glucose carbons into non-glycolytic pathways such as the HBP, glycogen and the PPP. In concert, cMPC1$^{-/-}$ hearts develop increased FAO and ketone body oxidation capacity, which could support mechanisms by which KDs or HFDs rescue their structural remodelling. A dramatic reduction in the accumulation of pyruvate, lactate and glycogen storage correlated with reversal of structural remodelling on KDs or HFDs. This raises the possibility that mechanisms for cardiotoxicity could arise from accumulation of glucose-derived intermediates (for example, *O*-GlcNAc and glycogen) and, potentially, tissue acidosis secondary to increased lactate.

An HFD was as effective as a KD in reversing cardiac remodelling in cMPC1$^{-/-}$ hearts, whereas a KE diet, which selectively increased ketone body availability, had an attenuated effect. It is possible that the level of hyperketonemia after KE feeding might not have been elevated enough to overcome the CAC defect in cMPC1$^{-/-}$ hearts. Our observations that increasing the availability of ketones or fatty acid substrates by dietary manipulation could prevent or reverse LV remodelling in non-stressed cMPC1$^{-/-}$ hearts suggests that increasing the availability of alternative carbon sources could ameliorate the pathophysiologic consequences of altered CAC function or pyruvate partitioning in cMPC1$^{-/-}$ hearts. This is supported by our observation that protection by KD feeding in cMPC1$^{-/-}$ hearts was dependent on the continuity of KD feeding (Extended Data Fig. 7). Additional mechanisms by which KDs or HFDs reverse cardiac structural, molecular and functional remodelling induced by MPC deficiency in non-stressed hearts should also be considered. For example, in addition to metabolic changes such as increased ketone oxidation and FAO, KDs may also mediate some of their effect via alternative mechanisms such as epigenetic changes that alter myocardial gene expression[49,50].

Normal hearts initially develop compensated cardiac hypertrophy after acute PO and this adaptation to PO requires energetic adaptations to the increased energy demand. As discussed above, increased anaplerosis via pyruvate carboxylation from both ME1 and PC is an important aspect of this adaptation. Without

a functional MPC, entry of pyruvate into the CAC by alternative mechanisms that exist in cMPC1$^{-/-}$ hearts is preferentially partitioned to PDC rather than entering the CAC pool as OAA or malate. Thus, the high energy demand induced by PO does not appear to be supported by increased ME1 flux into anaplerosis, leading to the rapid failure of MPC-deficient hearts. The failure of short-term KD to rescue cMPC1$^{-/-}$ hearts when subjected to PO identifies an indispensable requirement for MPC-delivered pyruvate to support CAC flux in the face of pathologic stress. However, a long-term KD leads to adaptations that reverse age-dependent ventricular remodelling via molecular and metabolic mechanisms discussed above. These adaptations restore the ability of cMPC1$^{-/-}$ hearts to respond to an added hemodynamic stress such as PO. Thus, the protective impact of a KD to restore the adaptive response to PO does not depend solely on the immediate availability of this alternative substrate, but also depends on the reversal of pathogenic and molecular abnormalities that require a longer time course to regress.

Although the protection by KD feeding in cMPC1$^{-/-}$ hearts was dramatic, a protective role for KD in murine models of HF remains to be definitively resolved. The mild protection of KD feeding on a HF model induced by TAC + myocardial infarction was published recently[51]. Fatty acid oxidation rates in murine models of PO-induced HF in mice are reported to be reduced or unchanged and remain repressed when these hearts are exposed to a more readily oxidized substrate such as ketones[8]. This contrasts with cMPC1$^{-/-}$ hearts that reveal increased utilization of fatty acids and ketones. Additional metabolic changes in the pressure-overloaded heart are also distinct from what was observed in the compensated hypertrophy stage in cMPC1$^{-/-}$ mice. For example, PO is characterized by elevated anaplerosis via the carboxylation of pyruvate mediated by ME1 (refs. [5,41]). In rodents and humans with HF, ME1 expression is induced[41], which contrasts with cMPC1$^{-/-}$ hearts in which ME1 expression was unchanged. Although a mismatch between glycolysis and glucose oxidation has been described after TAC, increasing ketone body utilization does not reverse this pattern[8]. This contrasts with cMPC1$^{-/-}$ mutants, which exhibit regression of HF and LV remodelling in concert with reduced accumulation of glycolytic intermediates, and an overall increased dependence on FAO on a KD. Taken together, these observations make it unlikely that altered MPC expression or function can account for the metabolic characteristics of pressure-overloaded (TAC) hearts or the partial effect of KDs on murine hearts after TAC.

In conclusion, despite evidence for short-term adaptive mechanisms by which glucose-derived carbons could enter the CAC in cMPC1$^{-/-}$ hearts, these hearts inexorably progress to HF and this inevitable cardiac dysfunction can be prevented by dramatically increasing the delivery of fatty acids and ketones. We identify a conserved role for mitochondrial pyruvate uptake in the myocardium to mobilize glycolysis-derived pyruvate for mitochondrial metabolism. Our findings are supported by two companion articles[52,53] indicating that loss of MPC in the heart results in age-related dilated cardiomyopathy, which is associated with redirection of glycolytic intermediates into metabolic pathways such as the pentose phosphate and serine biosynthetic pathways, which correlate with adverse LV remodelling. Moreover, they demonstrate that increasing the availability of alternative substrates by a ketogenic diet or HFD, or by increasing pyruvate mobilization into the TCA by inducibly increasing the expression of MPC in an HF model, reverses or attenuates LV remodelling. Thus, without MPC-mediated pyruvate uptake, the accumulation of potentially toxic glycolytic intermediates and their metabolic byproducts are likely to contribute to the maladaptive pathologic hypertrophy, leading to age-dependent HF or accelerated HF in response to a hemodynamic stress. Complete inhibition of glycolysis and prevention of glycolytic metabolite accumulation by feeding alternative substrates parallel the reversal or prevention of LV remodelling.

Methods

Animal experiments and generation of cardiomyocyte-restricted MPC1 knockout mice. Animal work was performed in accordance with protocols approved by the University of Iowa Institutional Animal Care and Use Committee. Mice were maintained on rodent diet and water available freely in a vivarium with a 12-h light–dark cycle at 22 °C and 30–70% humidity. MPC1 cardiomyocyte-restricted knockout mice (cMPC1$^{-/-}$) were generated by interbreeding MPC1$^{flox/flox}$ mice with mice hemizygous for Cre recombinase, under control of the *MYH6* promoter, which results in the recombination of the LoxP sites and removal of exons 3–5. Experimental cohorts were generated by crossing MPC1$^{flox/flox}$ and MPC1$^{flox/+}$:αMHC-Cre mice to generate Mpc1$^{flox/flox}$:αMHC-Cre (cMPC1$^{-/-}$) and Mpc1$^{flox/flox}$ (WT) littermates, which were used as controls. For the KD study, mice were fed with Teklad 2920X diet (control chow) or KD (Bio-Serv, AIN-76A-Modified). For HFD feeding, the normal chow diet (NCD) (D12450J) and HFD (D12492) were purchased from Research Diets, and the KE chow was prepared by Research Diets using 2920X mixed with the 10% (v:w) *R*,*S*-butanediol diacetoacetate (KE) purchased from Keto Research Chemicals. The KE diet was supplemented with the addition of 200 mM potassium β-HB to the drinking water.

Transmission electron microscopy. LV tissue was isolated and cut into small pieces (<1 mm^3) and fixed with 2.5% glutaraldehyde (in 0.1 M sodium cacodylate buffer, pH 7.4) overnight at 4 °C and then post-fixed with 1% osmium tetroxide for 1 h. After serial alcohol dehydration (50%, 75%, 95% and 100%), the samples were embedded in Epon 12 (Ted Pella). Ultramicrotomy was performed and ultrathin sections (70 nm) were post-stained with uranyl acetate and lead citrate. Samples were examined with a JEOL 1230 transmission electron microscope. Mitochondrial volume density, number and size were quantified using a grid system.

Echocardiography. Transthoracic echocardiograms were acquired from sedated (midazolam 0.1 mg subcutaneous injection) mice. The anterior chest hair was removed with Nair (Church & Dwight) and warmed gel was applied. The mouse was held gently by the nape of the neck and positioned in the left lateral position. Cardiac images were obtained via a 30-MHz linear array transducer applied to the chest. The transducer was coupled to a Vevo 2100 imager (VisualSonics). Images of the short and long axis were obtained with a frame rate of ~180–250 Hz. All image analysis was performed offline using Vevo 2100 analysis software (v.1.5). Endocardial and epicardial borders were traced on the short axis view in diastole and systole. LV length was measured from endocardial and epicardial borders to the LV outflow tract in diastole and systole. The biplane area–length method was then performed to calculate LV mass and ejection fraction.

Mitochondrial pyruvate uptake. Mitochondria were isolated in buffer containing 70 mmol l^{-1} of sucrose, 210 mmol l^{-1} of D-mannitol, 1 mmol l^{-1} of (ethylenebis(oxonitrilo))tetra-acetate (EGTA), 0.5% fatty acid-free bovine serum albumin (BSA) and 5 mmol l^{-1} of 4-(2-hydroxyethyl)-1-piperazine-ethanesulfonic acid (Hepes), pH 7.2. Mitochondria were resuspended in 100 µl of uptake buffer (120 mmol l^{-1} of KCl, 5 mmol/ l^{-1} of KH_2PO_4, 1 mmol l^{-1} of EGTA, 5 mmol l^{-1} of Hepes, pH 7.4, 1 µmol l^{-1} of rotenone and 1 µmol l^{-1} of antimycin A) and were aliquoted into two 30-µl aliquots. One aliquot was treated with 2 mM α-cyano-4-hydroxycinnamic acid (CHC, Sigma-Aldrich, catalogue no. 476870) and the other was treated with a volume of uptake buffer equal to the volume of CHC added. The remaining untreated resuspension was used to perform a protein assay for normalization. Of the treated mitochondria, 30 µl was rapidly mixed with 30 µl of 2× pyruvate buffer (uptake buffer, pH 6.1, containing 0.1 mM [2-^{14}C]pyruvate (Perkin Elmer, catalogue no. NEC256050UC)), generating the pH gradient needed to initiate uptake. The final concentration of [^{14}C]pyruvate was 0.05 mM. Stop buffer (uptake buffer, pH 6.8, supplemented with 10 mmol l^{-1} of CHC), 100 µl, was added to halt uptake 60 s after uptake was initiated. Mitochondria were recovered by passing the solution through a 0.8-µm cellulose filter (Millipore, catalogue no. AAWP-142-50) and a 0.45-µm nitrocellulose filter (Bio-Rad, catalogue no. 162-0115). Filters were washed twice with 200 µl of wash buffer (uptake buffer, pH 6.8, supplemented with 2 mmol l^{-1} of CHC and 5 mmol l^{-1} of pyruvate) and placed into scintillation vials for quantification. The assays were conducted with all buffers and reaction vessels cooled to 4 °C and maintained throughout the assay period on wet ice. Mitochondria pre-treated with CHC were used as a negative control and counts were subtracted from non-pre-treated mitochondria. Although rotenone and antimycin A are included in the assay buffer to ablate electron transport chain activity, limited pyruvate oxidation via PDH or other metabolic reactions may occur during the assay, until the cofactors have been depleted or through trace residual electron transport chain activity. However, because of the proton gradient experimentally generated by the ΔpH of 0.6 units between the mitochondria and the extra-mitochondrial pyruvate-containing media, pyruvate uptake, which is proton dependent, is expected to remain rate limiting during the linear phase of the pyruvate uptake assay. In the event of limited pyruvate oxidation, the use of 2-[^{14}C] pyruvate ensures that ^{14}C persists within mitochondria for a full turn of the CAC cycle. Therefore, ^{14}C counts were interpreted as mitochondrial pyruvate uptake.

Mitochondrial respiration. Fresh whole hearts were used to isolate mitochondria. Mitochondria were isolated in buffer containing 70 mmol $^{-1}$ of

sucrose, 210 mmol l^{-1} of D-mannitol, 1 mmol l^{-1} of EGTA, 0.5% fatty acid-free BSA and 5 mmol l^{-1} of Hepes, pH 7.2. Mitochondria were resuspended and protein concentration was determined using the Bradford method (Thermo Fisher Scientific, 23236). Oxygen consumption rate (OCR) measurements were performed in isolated mitochondria using the Seahorse XFe24 (Agilent) according to the manufacturer's instructions. Mitochondria were loaded into plates for the assays at a concentration of 10 µg per well. Isolation buffer was replaced by pre-warmed, unbuffered Dulbecco's modified Eagle's medium (Sigma) and equilibrated for 1 h at 37 °C. Oligomycin (2 µmol l^{-1}), carbonyl cyanide-4-(trifluoromethoxy)phenylhydrazone (FCCP; 0.4 µmol l^{-1}), rotenone (0.5 µmol l^{-1}) and antimycin A (0.5 µmol l^{-1}) were dissolved in assay medium and loaded on sensor cartridge ports. Oxygen consumption was detected under basal conditions followed by the sequential addition of the indicated drugs.

Gene expression analysis. Hearts were excised, rinsed in ice-cold phosphate-buffered saline and snap-frozen. RNA from ventricular tissue was extracted using TRIzol (Life Technologies, catalogue no. 15596018). The RNA was quantified with a Nanodrop 2000 Spectrophotometer (Thermo Fisher Scientific). Complementary DNA was generated with the High-Capacity cDNA Reverse Transcription Kit (Applied Biosystems, catalogue no. 4368814) using the oligo(dT)12–18 primer (Thermo Fisher Scientific) and analysed by real-time PCR using SYBR green chemistry (Thermo Fisher Scientific, catalogue no. 4367659). Primers were designed using Primer-BLAST[54] and are listed in Supplementary Table 1. Quantitative (q)PCR standard curves were plotted using serial dilutions of cDNA of the analysed samples. At least four dilution points were used to plot the standard curve and the efficiency of all primer sets was between 80% and 120%. The housekeeping gene *RP16S* was used as an internal control for cDNA quantification and normalization of the amplified products. All data are reported as mean ± s.e.

Immunoblot analysis. Heart tissue was homogenized in radioimmunoprecipitation assay buffer (50 mmol l^{-1} of Tris-HCl, pH 8.0, 150 mmol l^{-1} of NaCl, 0.5% sodium deoxycholate, 0.1% sodium dodecylsulfate, 1.0% NP-40) with 1× protease inhibitor (Thermo Fisher Scientific, catalogue no. 78440). Homogenates were incubated on ice for 30 min and centrifuged at 16,000*g* before the supernatants were collected. Protein concentration was determined using the BCA kit (Thermo Fisher Scientific, catalogue no. 23225). Proteins were separated by Tris-glycine gels, transferred to a 0.22-µm poly(vinylidene difluoride) membrane (Millipore, catalogue no. IPVH00010), and blocked with TBST (50 mmol^{-1} of Tris, 150 mmol l^{-1} of NaCl and 0.05% Tween-20) supplemented with 5% non-fat dry milk (Bio-Rad, catalogue no. 1706404XTU), incubated with primary antibodies at 4 °C overnight and fluorescent secondary antibodies (Cell Signaling Technology, catalogue nos. 5366 and 5257) for 1 h, and visualized using the LiCor Odyssey CLx system (LI-COR Biotechnology). Primary antibody information is listed in Supplementary Table 2.

In situ metabolomics. Heart samples were freeze-clamped and stored at −80 °C. Frozen tissue was lyophilized overnight and then extracted in 720 µl of methanol, acetonitrile and water in a 2:2:1 ratio. The standard mixture (1 mg ml^{-1} of D$_4$-succinate, D$_8$-valine, D$_4$-citrate, [$^{13}C_5$]glutamine, [$^{13}C_5$]glutamate, [$^{13}C_6$]lysine, [$^{13}C_5$]methionine, [$^{13}C_3$]serine and [$^{13}C_{11}$]tryptophan) was added into the extraction buffer at a 1:1,000 ratio before use. Tissues were placed in tubes with ceramic beads and extracted using a Bead Mill Homogenizer (Bead Ruptor Elite, Omni International) at 6.45 m s^{-1} for 30 s. After rotating at −20 °C for 1 h, sample tubes were centrifuged at 21,000*g* for 10 min and then the supernatant (~400 µl) was transferred to a new tube to dry at room temperature in a Savant SPD131DDA SpeedVac Concentrator (Thermo Fisher Scientific).

For LC/MS, 40 µl of acetonitrile:water (1:1) was added into the completely dried samples and vortexed to completely dissolve. After centrifuging at 21,000*g* for 5 min, supernatants were transferred to the LC tube for the assay. LC/MS-based analyses were performed on a Millipore SeQuant ZIC-pHILIC (2.1 × 150 mm^2, 5-µm particle size) with a ZIC-pHILIC guard column (20 × 2.1 mm^2, Sigma-Aldrich) coupled to a Thermo Q Exactive Hybrid Quadrupole Orbitrap mass spectrometer with a Vanquish Flex UHPLC system (Thermo Fisher Scientific). The chromatographic gradient was run at a flow rate of 0.150 ml min^{-1} as follows: 0–20 min—linear gradient from 80% to 20% buffer B (CH_3CN, mixed with 20–80% of buffer A: 20 mmol l^{-1} of ammonium carbonate and 0.1% ammonium hydroxide, respectively); 20–20.5 min—linear gradient from 20–80% buffer B; and 20.5–28 min—hold at 80% buffer B. The MS was operated in full-scan, polarity-switching mode, with the spray voltage set to 3.0 kV, the heated capillary held at 275 °C and the HESI probe held at 350 °C. The sheath gas flow was set to 40 units, the auxiliary gas flow was set to 15 units and the sweep gas flow was set to 1 unit. MS data acquisition was performed in a range of m/z of 70–1,000, with the resolution set at 70,000, the automatic gain control (AGC) target at 1×10^6 and the maximum injection time at 20 ms.

For GC/MS, samples were derivatized using a combination of methoxyamine and pyridine (MOX solution). MOX solution was made by adding methoxyamine in anhydrous pyridine to achieve 11.4 mg ml^{-1}. The pyridine was extracted from the bottle under a continuous flow of nitrogen using a dry syringe and a nitrogen adaptor. Of the MOX solution, 30 µl was added into the dried extracts, vortexed for 10 min and followed by heating at 60 °C for 1 h. Then, 20 µl of *N*-methyl-*N*-(trimethylsilyl)-trifluoroacetamide reagent was added to the 30 µl of solution, vortexed for 1 min and heated at 60 °C for 30 min. The GC/MS data were acquired using a Trace 1310 Gas Chromatograph (Thermo Fisher Scientific) coupled with an ISQ LT Single Quadrupole mass spectrometer (Thermo Fisher Scientific). GC was performed using a TraceGOLD TG-5SilMS GC Column (30 m × 0.25 mm inner diameter, coated with a 0.25-µm film, Thermo Fisher Scientific). The GC conditions were as follows: initial oven temperature of 80 °C held for 3 min, followed by a temperature ramp of 20 °C min^{-1} to 280 °C, with a final hold at 280 °C for 8 min. Helium was used as a carrier gas with a flow rate of 1.2 ml min^{-1}. The MS was operated by electron impact ionization at 70 eV and the scan mode was selected ion monitoring.

For both LC/MS and GC/MS, data were collected using Xcalibur Software (Thermo Fisher Scientific). Metabolite peak detection was performed by TraceFinder General Quant (Thermo Fisher Scientific). Metabolites were identified using an in-house library developed from purchased standards. Metabolomics data were analysed by MetaboAnalyst (http://www.metaboanalyst.ca)[55].

Isolated working heart perfusion. Langendorff heart perfusion was initially prepared as previously described[56]. In brief, hearts from WT and cMPC1$^{-/-}$ mice were excised after isoflurane anaesthesia, and then cannulated and retrogradely perfused with modified Krebs–Henseleit buffer (118.5 mmol l^{-1} of NaCl, 4.7 mmol l^{-1} of KCl, 2 mmol l^{-1} of $CaCl_2$, 1.2 mmol l^{-1} of $MgSO_4$, 1.2 mmol l^{-1} of KH_2PO_4 and 17.3 mM $NaHCO_3$). After a stable perfusion for 5 min, the perfusion line was switched to the working heart mode (preload at 10 mmH_2O and afterload at 60 mmH_2O) with modified Krebs–Henseleit buffer equilibrated with 95% O_2/5% CO_2, containing 0.4 mmol l^{-1} of palmitate bound to BSA in a 3:1 ratio, 5 mmol l^{-1} of glucose, 0.5 mmol l^{-1} of sodium pyruvate and 1 mmol l^{-1} of sodium lactate. Buffer temperature was maintained at 39 °C. Glucose oxidation and glycolysis were measured in one cohort of perfused hearts, and palmitate oxidation was measured in the second cohort. Glucose oxidation was determined by capturing $^{14}CO_2$ released from the oxidation of [U-$^{14}C_6$]glucose (PerkinElmer, specific activity, 296 MBq mol^{-1}). Glycolytic flux was measured by the amount of ^3H_2O released from the metabolism of exogenous [5-^{3}H]glucose (PerkinElmer, specific activity, 177 MBq mol^{-1}). Palmitate oxidation was assessed from the amount of ^3H_2O oxidized from the [9,10-$^3H_2$]palmitate (PerkinElmer, specific activity 42 GBq mol^{-1}).

The perfusion lasted for 1 h and buffer samples were collected from the circulating system every 20 min. Cardiac function, including heart rate (in beat min^{-1}) and developed pressure (DevP, in mm Hg), was monitored by a Millar pressure catheter (Millar Instruments). Oxygen content and coronary flow were recorded every 20 min throughout the 1-h perfusion. The oxygen content of freshly oxygenated buffer (arterial partial pressure of oxygen (PaO_2)) and oxygen concentration in the pulmonary artery effluent (venous partial pressure of oxygen (PvO_2)) were collected using a capillary tube and measured using a fiberoptic oxygen sensor (Ocean Optics). Myocardial O_2 consumption (MVO_2), cardiac hydraulic work (CHW) and cardiac efficiency (CE) were calculated using the following formulae. MVO_2, in µmol min^{-1} g^{-1} of dry heart weight (DHW), was determined as follows: $MVO_2 = ((PaO_2 - PvO_2)/100) \times (\text{coronary flow/DHW}) \times 0.0393 \times (1{,}000 \times C)$, where PaO_2 is the arterial partial pressure of oxygen in mmHg, PvO_2 the venous partial pressure of oxygen in mmHg and C the Bunsen coefficient for plasma, that is, 0.0212. MVO_2 (ml min^{-1}) was converted to µmol min^{-1} by multiplying by the conversion factor 0.0393. Cardiac hydraulic work (CHW), in J min^{-1} g^{-1} of wet heart weight (WHW), was determined as follows: $CHW = (CO \times DevP \times 1.33 \times 10^{-4})$ per g WHW, where CO is the cardiac output in ml min^{-1}. Cardiac efficiency (CE), as a percentage, was determined as follows: $CE = CHW/MVO_2 \times 100$.

MVO_2 (ml min^{-1}) was converted to µmol min^{-1} by multiplying by the conversion factor 0.0393 and then to J min^{-1} using the conversion formula of 1 µmol O_2 = 0.4478 J.

Metabolite concentration and ^{13}C-labelled flux analysis by GC/MS. GC/MS was performed to measure the tissue concentration and ^{13}C-labelled enrichment of CAC intermediates, pyruvate, lactate and intracellular free amino acids as described previously[37,57]. Hearts from both control and cMPC1$^{-/-}$ mice were perfused retrogradely through the aorta at a constant pressure of 70 mmHg with a non-recirculating modified Krebs buffer containing (in mmol l^{-1}): 118.5 NaCl, 4.7 KCl, 1.5 $CaCl_2$, 1.2 KH_2PO_4, 1.2 $MgSO_4$, 17.3 mM $NaHCO_3$, pH 7.4 and various substrates (in mmol l^{-1}: glucose 10, lactate 0.5, palmitate-bound BSA 0.4, β-HB 0.1, glutamine 0.5, pyruvate 0.2). Cardiac function was monitored by LabChart system using a Millar catheter connected to a balloon filled with water. The balloon was inserted into the left ventricle and the diastolic pressure was set to 5–10 mmHg. Hearts were perfused with unlabelled substrates, freeze-clamped and extracted with 70% methanol and 1 mol l^{-1} of hydroxylamine, pH 7.6. Tissue lysate was mixed with the mixture containing internal and external standards. The mixture of organic acid (OA) standards included 200 nmol of [$^{13}C_3$]lactic acid, 60 nmol of [$^{13}C_3$]pyruvic acid, 30 nmol of [$^{13}C_4$]β-HB, 20 nmol of α-[$^{13}C_4$]ketobutyric acid, 20 nmol of citrate, 20 nmol of α-[$^{13}C_4$]KG, 20 nmol of D$_4$-succinate and 20 nmol of D$_3$-malate. The mixture of amino acid (AA) external standards included: [$^{13}C_3$]alanine, [$^{13}C_2$]glycine, [$^{13}C_5$]valine, [$^{13}C_6$,^{15}N]leucine, [$^{13}C_6$]isoleucine, [$^{13}C_5$,^{15}N]

proline, [$^{13}C_5$]methionine, [$^{13}C_5$,^{15}N]serine, [$^{13}C_4$,^{15}N]threonine, D$_5$-phenylalanine, [$^{13}C_4$,^{15}N]aspartate, [$^{13}C_5$,^{15}N]glutamate, [$^{13}C_6$]arginine, [$^{13}C_9$]tyrosine and [$^{13}C_6$]histidine. Samples were homogenized with 2.8-mm zirconium oxide beads (Omni International). Lysates were added with 1 mol l^{-1} of hydrochloric acid (pH between 5 and 6) to incubate at 70 °C for 15 min and then centrifuged at 22,000*g* for 10 min. The supernatant was evaporated, rinsed once with 100% methanol and drained twice with ammonium sulfate. After a quick centrifugation at 7,000*g*, the supernatant was evaporated again, samples were solubilized in 100% pyridine at 45 °C for 90 min and followed by derivatization using *N*-methyl-*N*-*tert*-butyldimethylsilyltrifluoroacetamide at 90 °C for 4 h. Samples were injected into an Agilent 6890N chromatograph coupled to a 5975N mass spectrometer operated in electronic ionization mode (helium gas) at a flow rate maintained throughout (OA 23.3 ml min^{-1} and AA 20.1 ml min^{-1}) in split mode (OA 28:1; AA 23.2:1). The temperature program for OAs was fixed as follows: 150 °C for 5 min, increment of 10 °C min^{-1} up to 300 °C, and then 20 °C min^{-1} up to 320 °C. For AAs, the temperature program was set as: 150 °C for 3 min, increment of 7 °C min^{-1} up to 210 °C and maintained constant for 3 min, increment of 7 °C min^{-1} up to 310 °C and maintained for 3 min, and then 10 °C min^{-1} up to 320 °C. Metabolites were identified according to the *m*/*z* and retention time, and quantified using internal or external standards and standard curves.

For ^{13}C-labelling experiments, unlabelled glucose or glutamine was replaced by [U-$^{13}C_6$]glucose or [U-$^{13}C_5$]glutamine, respectively. The perfusate was gassed with 5% CO_2:95% O_2. The hearts were perfused with unlabelled substrates for 15 min to reach stabilization and then the buffer was switched to the labelled substrate and the perfusion continued for 30 min. Hearts were freeze-clamped and saved immediately after perfusion and analysed via GC/MS. Procedures for determination of concentrations and ^{13}C labelling of metabolites (citrate, OAA, α-KG, succinate, malate, fumarate, pyruvate, lactate, alanine and serine) were performed as previously described[57] with slight modifications. Briefly, metabolites were extracted from pulverized heart powder using 70% methanol. The ^{13}C labelling of the OAA^{CIT} was assessed as previously described[37].

The absolute concentrations and ^{13}C enrichment of pyruvate, lactate, amino acids (alanine, serine, glutamate, glutamine, leucine, isoleucine and valine) and CAC intermediates (citrate, α-KG, succinate, fumarate and malate) in the extracted tissue were measured by GC/MS using an Agilent 6890N gas chromatograph equipped with a HP-5 column coupled to a 5975N mass spectrometer (Agilent Technologies) as described previously[56]. Raw data were collected by GC/MSD ChemStation. Data are presented as MPE.

$\mathrm{MPE} = \frac{A_{M+i}}{(\sum A_{M+i})} \times 100$, where A represents the peak area of each fragmentogram, measured by computer integration and corrected for naturally occurring heavy isotopes and i ranges from 0 to n, where n stands for the number of carbon atoms. Mass isotopomers of metabolites containing 1 to n ^{13}C-labelled atoms were identified as M+i, with $i = 1, 2, \ldots, n$.

The relative contribution of pyruvate to the formation of citrate via decarboxylation to acetyl-CoA (PDC) and via carboxylation (PC) to OAA or malate (via PC- or NADP$^+$-linked malic enzyme, respectively) is expressed relative to CS and was assessed from the ^{13}C labelling of tissue citrate, OAA^{CIT}, pyruvate and succinate as previously described in detail[56]. The percentage ^{13}C-labelled citrate recycling into the CAC (percentage citrate recycling) was estimated as previously reported[25,37].

Briefly, the equations of PDC/CS and PC/CS were listed as equations (1) and (2), respectively. *Fc* represents the fractional enrichment of the product derived from the preceding substrate.

$$\frac{\mathrm{PDC}}{\mathrm{CS}} = \left(Fc_{\mathrm{PYR}\rightarrow\mathrm{AC(CIT)}}\right) = \left(Fc_{\mathrm{PYR}\rightarrow\mathrm{AC}}\right) \times \left(Fc_{\mathrm{AC}\rightarrow\mathrm{CIT}}\right) = \frac{\mathrm{OAA}^{\mathrm{CIT}}_{\mathrm{M+2}}}{\mathrm{PYR}_{\mathrm{M+3}}} \quad (1)$$

$$\frac{\mathrm{PC}}{\mathrm{CS}} = \left(Fc_{\mathrm{PYR}\rightarrow\mathrm{OAA}}\right) \times \left(Fc_{\mathrm{OAA}\rightarrow\mathrm{CIT}}\right) = \frac{\mathrm{OAA}^{\mathrm{CIT'}}_{\mathrm{M+3}}}{\mathrm{PYR}_{\mathrm{M+3}}} \quad (2)$$

The M+3 OAA$^{CIT'}$ was calculated as

$$\mathrm{OAA}^{\mathrm{CIT'}}_{\mathrm{M+3}} = \text{measured } \mathrm{OAA}^{\mathrm{CIT}}_{\mathrm{M+3}} - \frac{\mathrm{OAA}^{\mathrm{PR}}_{\mathrm{M+3}}}{\mathrm{DF}} \quad (3)$$

The dilution factor (DF) and M+3 OAA^{PR} were calculated as equations (4) and (5), respectively.

$$\mathrm{DF} = \frac{\left[\mathrm{CIT}_{\sum M_i} - \left(\sum fi \times \mathrm{OAA}^{\mathrm{CIT}}_{\mathrm{M+1}}\right)\right]}{\left[\mathrm{SUC}_{\sum M_i}\right]} \quad (4)$$

$$\mathrm{OAA}^{\mathrm{PR}}_{\mathrm{M+3}} = \left[\tfrac{1}{2} \times (\mathrm{AC}_{\mathrm{M+2}} \times \mathrm{OAA}_{\mathrm{M+1}})\right] + \left[\tfrac{2}{3} \times (\mathrm{AC}_{\mathrm{M+2}} \times \mathrm{OAA}_{\mathrm{M+2}})\right] + \left[\tfrac{1}{2} \times (\mathrm{AC}_{\mathrm{M+2}} \times \mathrm{OAA}_{\mathrm{M+3}})\right] + \left[\tfrac{1}{2} \times (\mathrm{AC}_{\mathrm{M+1}} \times \mathrm{OAA}_{\mathrm{M+3}})\right] + \left[(\mathrm{AC}_{\mathrm{M+1}} \times \mathrm{OAA}_{\mathrm{M+4}})\right] \quad (5)$$

The percentage citrate recycling was calculated as

$$\text{Percentage citrate recycling} = \frac{\frac{\mathrm{OAA}^{\mathrm{PR}}_{\mathrm{M+3}}}{\mathrm{DF}}}{\text{Measured OAA}\,\frac{\mathrm{CIT}}{\mathrm{M+3}}} \times 100 \quad (6)$$

In vitro NMR. Hearts from both control and cMPC1$^{-/-}$ mice were perfused retrogradely through the aorta at a constant pressure of 70 mmHg with a non-recirculating, modified Krebs buffer containing (in mmol l^{-1}) 118.5 NaCl, 4.7 KCl, 1.5 $CaCl_2$, 1.2 KH_2PO_4 and 1.2 $MgSO_4$, 17.3 mM $NaHCO_3$ (pH 7.4) and various substrates (in mmol l^{-1}): glucose 10, lactate 0.5, palmitate-bound BSA 0.4, β-HB 0.1, glutamine 0.5, pyruvate 0.2. The perfusate was gassed with 5% CO_2:95% O_2 and the water-filled balloon was inserted into the left ventricle and the pressure set to 5–10 mmHg. The hearts were perfused with unlabelled substrates for 15 min to reach stabilization, and then the buffer was switched to the labelled substrate and the perfusion continued for 30 min. Hearts were snap-frozen and saved immediately after perfusion. Perfused hearts were extracted with perchloric acid, lyophilized and reconstituted in deuterium oxide. High-resolution, proton-decoupled ^{13}C NMR spectra were collected from acid extracts of hearts perfused with ^{13}C-enriched substrates in a 14.1-T NMR system (Bruker Instruments). Analysis of glutamate isotopomers and isotopologues from in vitro ^{13}C NMR of acid extracts of myocardium perfused with ^{13}C-enriched substrates provided the ratio anaplerosis:CS (*y*) and the fractional ^{13}C enrichment of acetyl-CoA from β-[^{13}C]HB (*Fc*) entering the CAC cycle. The fractional ^{13}C enrichment of glutamate in myocardium was quantified by signal intensity relative to a standard ^{13}C NMR spectrum of 100 mmol l^{-1} of glutamate and quantification of tissue glutamate via ultraviolet spectrophotometry[42].

^{13}C-labelled metabolite analyses in perfused hearts by LC/MS. Lyophilized heart extracts from hearts perfused with 2,4-[$^{13}C_2$]-β-HB were analysed by LC/MS as previously reported[58]. Briefly, the analysis was performed using a Dionex Ultimate 3000 RSLC liquid chromatograph with a Thermo Q-Exactive Plus mass spectrometer equipped with a heated ESI source. Samples were injected and separated on a Luna aminopropyl (100 × 1 mm^2, 3 µl) column using mobile phases A (10 mM ammonium acetate/10 mM ammonium hydroxide in 95% water) and B (10 mM ammonium acetate/10 mM ammonium hydroxide in 95% acetonitrile). Separation was performed using binary gradient of 75% to 0% B for 45 min, then 0% B for 12 min and 75% B for 13 min at a flow rate of 50 µl min^{-1} and column temperature of 30 °C. The mass spectrometer was operated in negative mode (*m*/*z* 68–1,020) with optimized HESI source conditions: auxiliary gas 10, sweep gas 1, sheet gas flow at 35 (arbitrary unit), spray voltage −3 kV, capillary temperature 275 °C, S-lens RF 50 and auxiliary gas temperature 150 °C. The AGC target was set at 1×10^6 ions and resolution at 70,000. Before analysis, the mass spectrometer was calibrated to fully optimize mass accuracy performance. Before and after sample analysis, the quality control samples were analysed to ensure the high quality of the data. Samples within the sequence were injected in a randomized order to minimize the possibility of column carry-over. The RAW files were collected and converted into mzXML format using Xcalibur software. The mzXML files were divided into two groups and analysed using the X13CMS R package. Metabolites were identified based on the *m*/*z* and retention times compared with standard counterparts analysed using the same conditions. Data are presented as fractional enrichment.

Histology. Mouse hearts were fixed in 10% zinc formalin, embedded in paraffin, proportioned into 5-µm sections, and stained with hematoxylin and eosin and trichrome under standard protocols. Images were obtained using the Olympus BX-61 microscope and Leica Aperio Ariol Automated Slide Scanner (Leica Biosystems). Cardiac fibrosis area was quantified using ImageJ.

Glycogen assay. Heart tissue from control and cMPC1$^{-/-}$ mice was freeze-clamped and extracted in ice-cold 0.3 mol l^{-1} perchloric acid solution. The extract was incubated with and without amyloglucosidase (Sigma-Aldrich, catalogue no. A7095) in 50 mmol l^{-1} of acetate, pH 5.5 and 0.02% BSA. Absorbance at 340 nm was compared with a series of standard samples (0–80 mmol l^{-1} of glucose solution). Results are presented as glucose released from glycogen and normalized to tissue weight.

TAC. Mice were anaesthetised with ketamine or xylazine (100 mg kg^{-1} or 5 mg kg^{-1}, respectively) via intraperitoneal injection, intubated with a 20G poly(ethylene) tube and ventilated with a small rodent ventilator (Harvard Apparatus). An opening was created between the second and third intercostal spaces where the aortic arch could be visualized. TAC was performed by tightening a ligature with a 7/0 Prolene suture against a 27G needle. The sham group was subjected to the same procedure but not banded. The skin was closed using 6/0 Ethilon nylon sutures. Mice were then removed from the ventilator, extubated and anaesthesia stopped. After recovery, mice were administered buprenorphine (1 mg kg^{-1} subcutaneous injection) twice a day for 48 h.

Data analysis. All data are presented as mean ± s.e.m. Unpaired Student's *t*-tests were performed for the comparison of two groups (control and cMPC1$^{-/-}$ groups). Two-way analysis of variance (ANOVA) was performed to analyse the differences by genotype and chow across four groups (such as control and cMPC1$^{-/-}$ mice under regular chow and KD/HFD), followed by Tukey's multiple comparison test. Statistical analysis was performed using the GraphPad Prism software. For all analyses, a P value <0.05 was regarded as significantly different.

Reporting summary. Further information on research design is available in the Nature Research Reporting Summary linked to this article.

Data availability

All data, apart from the western blots, that support the findings of the present study are available from the corresponding author upon reasonable request. Source data for western blots are provided with this paper.

Received: 17 February 2020; Accepted: 3 September 2020;
Published online: 26 October 2020

References

1. Wende, A. R., Brahma, M. K., McGinnis, G. R. & Young, M. E. Metabolic origins of heart failure. *JACC Basic Transl. Sci.* **2**, 297–310 (2017).
2. Doenst, T., Nguyen, T. D. & Abel, E. D. Cardiac metabolism in heart failure: implications beyond ATP production. *Circ. Res.* **113**, 709–724 (2013).
3. Owen, O. E., Kalhan, S. C. & Hanson, R. W. The key role of anaplerosis and cataplerosis for citric acid cycle function. *J. Biol. Chem.* **277**, 30409–30412 (2002).
4. Des Rosiers, C., Labarthe, F., Lloyd, S. G. & Chatham, J. C. Cardiac anaplerosis in health and disease: food for thought. *Cardiovasc. Res.* **90**, 210–219 (2011).
5. Pound, K. M. et al. Substrate-enzyme competition attenuates upregulated anaplerotic flux through malic enzyme in hypertrophied rat heart and restores triacylglyceride content: attenuating upregulated anaplerosis in hypertrophy. *Circ. Res.* **104**, 805–812 (2009).
6. Lommi, J. et al. Blood ketone bodies in congestive heart failure. *J. Am. Coll. Cardiol.* **28**, 665–672 (1996).
7. Aubert, G. et al. The failing heart relies on ketone bodies as a fuel. *Circulation* **133**, 698–705 (2016).
8. Ho, K. L. et al. Increased ketone body oxidation provides additional energy for the failing heart without improving cardiac efficiency. *Cardiovasc. Res.* **115**, 1606–1616 (2019).
9. Huang, Y., Zhou, M., Sun, H. & Wang, Y. Branched-chain amino acid metabolism in heart disease: an epiphenomenon or a real culprit? *Cardiovasc. Res.* **90**, 220–223 (2011).
10. Marazzi, G., Rosanio, S., Caminiti, G., Dioguardi, F. S. & Mercuro, G. The role of amino acids in the modulation of cardiac metabolism during ischemia and heart failure. *Curr. Pharm. Des.* **14**, 2592–2604 (2008).
11. Drake, K. J., Sidorov, V. Y., McGuinness, O. P., Wasserman, D. H. & Wikswo, J. P. Amino acids as metabolic substrates during cardiac ischemia. *Exp. Biol. Med.* **237**, 1369–1378 (2012).
12. Allard, M. F., Schonekess, B. O., Henning, S. L., English, D. R. & Lopaschuk, G. D. Contribution of oxidative metabolism and glycolysis to ATP production in hypertrophied hearts. *Am. J. Physiol.* **267**, H742–H750 (1994).
13. Kagaya, Y. et al. Effects of long-term pressure overload on regional myocardial glucose and free fatty acid uptake in rats. A quantitative autoradiographic study. *Circulation* **81**, 1353–1361 (1990).
14. Karwi, Q. G., Uddin, G. M., Ho, K. L. & Lopaschuk, G. D. Loss of metabolic flexibility in the failing heart. *Front. Cardiovasc. Med.* **5**, 68 (2018).
15. Chandramouli, C. et al. Myocardial glycogen dynamics: new perspectives on disease mechanisms. *Clin. Exp. Pharm. Physiol.* **42**, 415–425 (2015).
16. Leong, H. S., Brownsey, R. W., Kulpa, J. E. & Allard, M. F. Glycolysis and pyruvate oxidation in cardiac hypertrophy—why so unbalanced? *Comp. Biochem Physiol. A Mol. Integr. Physiol.* **135**, 499–513 (2003).
17. Lopaschuk, G. D., Wambolt, R. B. & Barr, R. L. An imbalance between glycolysis and glucose oxidation is a possible explanation for the detrimental effects of high levels of fatty acids during aerobic reperfusion of ischemic hearts. *J. Pharm. Exp. Ther.* **264**, 135–144 (1993).
18. Nascimben, L. et al. Mechanisms for increased glycolysis in the hypertrophied rat heart. *Hypertension* **44**, 662–667 (2004).
19. Comte, B. et al. A 13C mass isotopomer study of anaplerotic pyruvate carboxylation in perfused rat hearts. *J. Biol. Chem.* **272**, 26125–26131 (1997).
20. Peuhkurinen, K. J., Nuutinen, E. M., Pietilainen, E. P., Hiltunen, J. K. & Hassinen, I. E. Role of pyruvate carboxylation in the energy-linked regulation of pool sizes of tricarboxylic acid-cycle intermediates in the myocardium. *Biochem. J.* **208**, 577–581 (1982).
21. Pisarenko, O. I., Solomatina, E. S. & Studneva, I. M. The role of amino acid catabolism in the formation of the tricarboxylic acid cycle intermediates and ammonia in anoxic rat heart. *Biochim. Biophys. Acta* **885**, 154–161 (1986).
22. Gibala, M. J., Young, M. E. & Taegtmeyer, H. Anaplerosis of the citric acid cycle: role in energy metabolism of heart and skeletal muscle. *Acta Physiol. Scand.* **168**, 657–665 (2000).
23. Opie, L. H. & Mansford, K. R. L. The value of lactate and pyruvate measurements in the assessment of the redox state of free nicotinamide-adenine dinucleotide in the cytoplasm of perfused rat heart. *Eur. J. Clin. Invest.* **1**, 295–306 (1971).
24. Lazo, P. A. & Sols, A. Pyruvate dehydrogenase complex of ascites tumour. Activation by AMP and other properties of potential significance in metabolic regulation. *Biochem. J.* **190**, 705–710 (1980).
25. Comte, B., Vincent, G., Bouchard, B. & Des Rosiers, C. Probing the origin of acetyl-CoA and oxaloacetate entering the citric acid cycle from the ^{13}C labeling of citrate released by perfused rat hearts. *J. Biol. Chem.* **272**, 26117–26124 (1997).
26. Bricker, D. K. et al. A mitochondrial pyruvate carrier required for pyruvate uptake in yeast, *Drosophila*, and humans. *Science* **337**, 96–100 (2012).
27. Halestrap, A. P. The mitochondrial pyruvate carrier: has it been unearthed at last? *Cell Metab.* **16**, 141–143 (2012).
28. Herzig, S. et al. Identification and functional expression of the mitochondrial pyruvate carrier. *Science* **337**, 93–96 (2012).
29. Vanderperre, B. et al. Embryonic lethality of mitochondrial pyruvate carrier 1 deficient mouse can be rescued by a ketogenic diet. *PLoS Genet.* **12**, e1006056 (2016).
30. Gray, L. R. et al. Hepatic mitochondrial pyruvate carrier 1 is required for efficient regulation of gluconeogenesis and whole-body glucose homeostasis. *Cell Metab.* **22**, 669–681 (2015).
31. McCommis, K. S. et al. Loss of mitochondrial pyruvate carrier 2 in the liver leads to defects in gluconeogenesis and compensation via pyruvate–alanine cycling. *Cell Metab.* **22**, 682–694 (2015).
32. Rauckhorst, A. J. et al. The mitochondrial pyruvate carrier mediates high fat diet-induced increases in hepatic TCA cycle capacity. *Mol. Metab.* **6**, 1468–1479 (2017).
33. Sharma, A. et al. Impaired skeletal muscle mitochondrial pyruvate uptake rewires glucose metabolism to drive whole-body leanness. *eLife* **8**, e45873 (2019).
34. Fernandez-Caggiano, M. et al. Analysis of mitochondrial proteins in the surviving myocardium after ischemia identifies mitochondrial pyruvate carrier expression as possible mediator of tissue viability. *Mol. Cell Proteom.* **15**, 246–255 (2016).
35. Abel, E. D. et al. Cardiac hypertrophy with preserved contractile function after selective deletion of GLUT4 from the heart. *J. Clin. Invest.* **104**, 1703–1714 (1999).
36. Krebs, H. A. & Gascoyne, T. The redox state of the nicotinamide-adenine dinucleotides in rat liver homogenates. *Biochem. J.* **108**, 513–520 (1968).
37. Ruiz, M., Gelinas, R., Vaillant, F., Lauzier, B. & Des Rosiers, C. Metabolic tracing using stable isotope-labeled substrates and mass spectrometry in the perfused mouse heart. *Methods Enzymol.* **561**, 107–147 (2015).
38. Halestrap, A. P. & Denton, R. M. The specificity and metabolic implications of the inhibition of pyruvate transport in isolated mitochondria and intact tissue preparations by alpha-cyano-4-hydroxycinnamate and related compounds. *Biochem. J.* **148**, 97–106 (1975).
39. Contreras-Baeza, Y. et al. Monocarboxylate transporter 4 (MCT4) is a high affinity transporter capable of exporting lactate in high-lactate microenvironments. *J. Biol. Chem.* **294**, 20135–20147 (2019).
40. Lindblom, P. et al. Isoforms of alanine aminotransferases in human tissues and serum: differential tissue expression using novel antibodies. *Arch. Biochem. Biophys.* **466**, 66–77 (2007).
41. O'Donnell, J. M., Kalichira, A., Bi, J. & Lewandowski, E. D. In vivo, cardiac-specific knockdown of a target protein, malic enzyme-1, in rat via adenoviral delivery of DNA for non-native miRNA. *Curr. Gene Ther.* **12**, 454–462 (2012).
42. Lahey, R. et al. Enhanced redox state and efficiency of glucose oxidation with miR based suppression of maladaptive NADPH-dependent malic enzyme 1 expression in hypertrophied hearts. *Circ. Res.* **122**, 836–845 (2018).
43. Funk, A. M. et al. Effects of deuteration on transamination and oxidation of hyperpolarized ^{13}C-pyruvate in the isolated heart. *J. Magn. Reson.* **301**, 102–108 (2019).
44. Brooks, G. A. The science and translation of lactate shuttle theory. *Cell Metab.* **27**, 757–785 (2018).
45. Chen, Y. J. et al. Lactate metabolism is associated with mammalian mitochondria. *Nat. Chem. Biol.* **12**, 937–943 (2016).
46. Taylor, E. B. Functional properties of the mitochondrial carrier system. *Trends Cell Biol.* **27**, 633–644 (2017).
47. Ferron, M., Denis, M., Persello, A., Rathagirishnan, R. & Lauzier, B. Protein *O*-GlcNacylation in cardiac pathologies: past, present, puture. *Front. Endocrinol.* **9**, 819 (2018).
48. Arad, M. et al. Glycogen storage diseases presenting as hypertrophic cardiomyopathy. *N. Engl. J. Med.* **352**, 362–372 (2005).
49. Puchalska, P. & Crawford, P. A. Multi-dimensional roles of ketone bodies in fuel metabolism, signaling, and therapeutics. *Cell Metab.* **25**, 262–284 (2017).
50. Ruan, H. B. & Crawford, P. A. Ketone bodies as epigenetic modifiers. *Curr. Opin. Clin. Nutr. Metab. Care* **21**, 260–266 (2018).
51. Horton, J. L. et al. The failing heart utilizes 3-hydroxybutyrate as a metabolic stress defense. *JCI Insight* **4**, e124079 (2019).
52. Fernandez-Caggiano, M. et al. Mitochondrial pyruvate carrier abundance mediates pathological cardiac hypertrophy. *Nat. Metabol.* https://doi.org/10.1038/s42255-020-00276-5 (2020).

53. McCommis, K. S. et al. Nutritional modulation of heart failure in mitochondrial pyruvate carrier–deficient mice. *Nat. Metabol.* https://doi.org/10.1038/s42255-020-00296-1 (2020).
54. Ye, J. et al. Primer-BLAST: a tool to design target-specific primers for polymerase chain reaction. *BMC Bioinform.* **13**, 134 (2012).
55. Chong, J., Wishart, D. S. & Xia, J. Using MetaboAnalyst 4.0 for comprehensive and integrative metabolomics data analysis. *Curr. Protoc. Bioinformatics* **68**, e86 (2019).
56. Riehle, C. et al. PGC-1β deficiency accelerates the transition to heart failure in pressure overload hypertrophy. *Circ. Res.* **109**, 783–793 (2011).
57. Vaillant, F. et al. Ivabradine and metoprolol differentially affect cardiac glucose metabolism despite similar heart rate reduction in a mouse model of dyslipidemia. *Am. J. Physiol. Heart Circ. Physiol.* **311**, H991–H1003 (2016).
58. Huang, X. et al. X13CMS: global tracking of isotopic labels in untargeted metabolomics. *Anal. Chem.* **86**, 1632–1639 (2014).

Acknowledgements

This work was supported by: American Heart Association (AHA; grant nos. 16SFRN31810000 to E.D.A. and 15POST22940024 to Y.Z.); Montreal Heart Institute Foundation (CDR); National Institutes of Health (NIH; grant nos. OD019941 to R.M.W., and R01 DK104998 and R00 AR059190 to E.B.T.); T32 (grant no. HL007638 to A.J.R.); American Diabetes Association (grant no. 1-18-PDF-060 (to A.J.R.); and NIH (grant nos. F32 DK101183 to L.R.G., U54DK110858, 1S10OD021505 and 1S10OD018210 to J.E.C., R01HL113057, R01HL132525 and R01HL049244 to E.D.L. and DK091538 to P.A.C.).

Author contributions

Y.Z. and E.D.A. designed the research. Y.Z., P.V.T., J.D.C., I.R.-F., J.M.M., J.S., A.D.P., F.T., L.M.T., A.J.R., L.R.G., P.P., T.R.F., R.M., K.Z., W.J.K., T.C., S.H., K.L., K.M.K., J.L.S., L.H., R.M.W. and J.E.C. performed the research. E.B.T. and J.R. provided materials and methodology support. Y.Z., E.D.L., P.A.C., C.D.R. and E.D.A. analysed the data. P.A.C., E.D.L. and C.D.R. contributed to the writing. Y.Z. and E.D.A. wrote the paper.

Competing interests

The authors declare no competing interests.

Additional information

Extended data is available for this paper at https://doi.org/10.1038/s42255-020-00288-1.

Supplementary information is available for this paper at https://doi.org/10.1038/s42255-020-00288-1.

Correspondence and requests for materials should be addressed to E.D.A.

Peer review information Primary Handling Editor: George Caputa.

Reprints and permissions information is available at www.nature.com/reprints.

Publisher's note Springer Nature remains neutral with regard to jurisdictional claims in published maps and institutional affiliations.

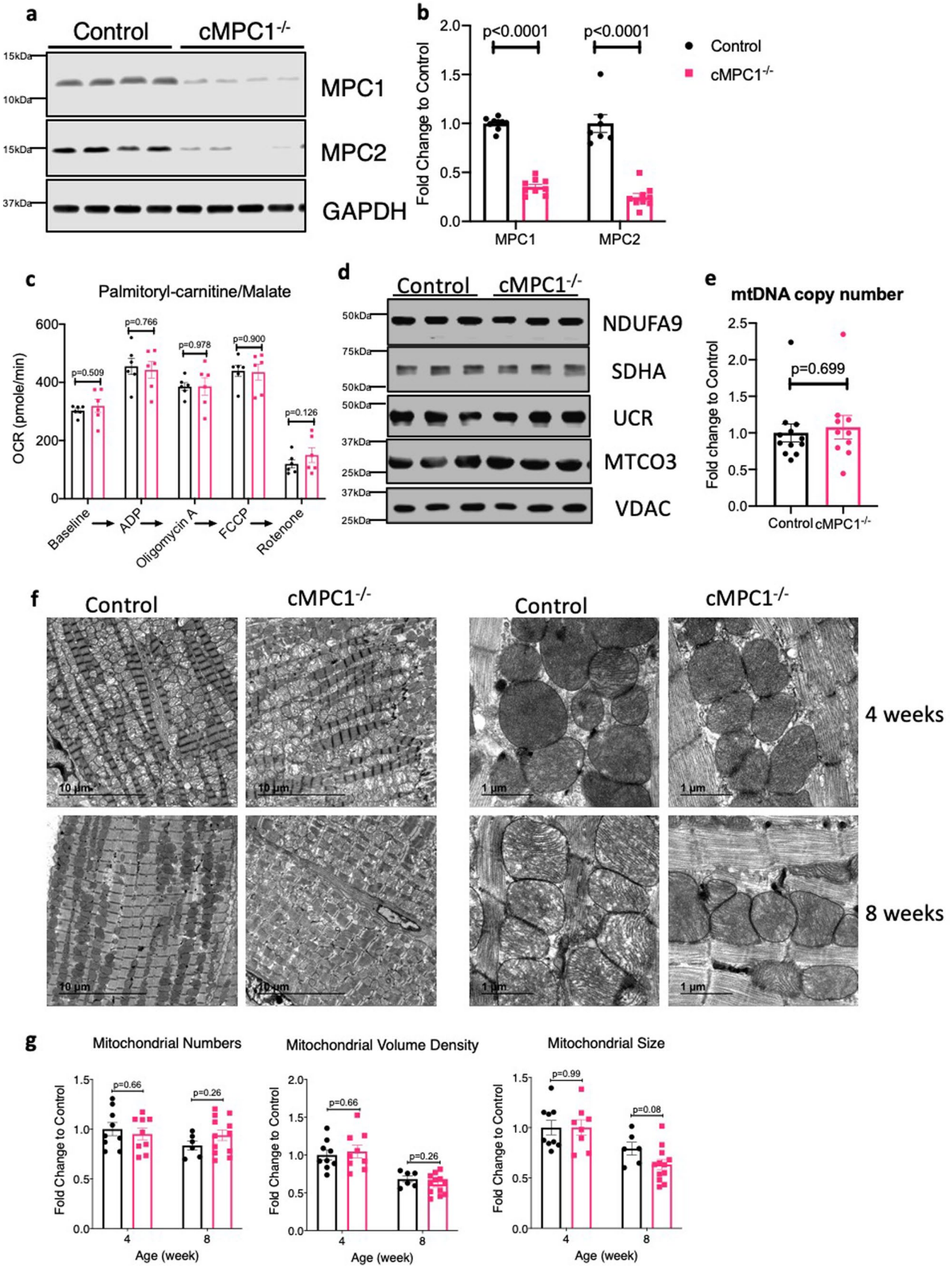

Extended Data Fig. 1 | See next page for caption.

Extended Data Fig. 1 | Mitochondrial Characterization of cMPC1$^{-/-}$ hearts. a, **b**, MPC protein levels were determined by Western blots in whole heart lysates from 4-week-old cMPC1$^{-/-}$ mice. Images are representative of n = 8 per group. **c**, Palmitoyl-carnitine driven oxygen consumption by seahorse respirometry in isolated mitochondria (n = 6 both groups). **d**, Expression of selected electron transport chain (ETC) subunits (from Complex I-V) and VDAC by Western blot in heart lysates from control and cMPC1$^{-/-}$ mice. Images are representative of n = 3 per group. **e**, mtDNA copy number determined by qPCR analysis and normalized to the nuclear gene RPL13A in 8-week-old cMPC1$^{-/-}$ hearts (Control, 12; cMPC1$^{-/-}$, 10). **f**, Representative TEM images of cMPC1$^{-/-}$ hearts from 4 and 8-week-old mice. Images are representative of n = 9 (4-week-old control and cMPC1$^{-/-}$)/6(8-week-old control)/12(8-week-old cMPC1$^{-/-}$). **g**, Quantification of mitochondrial number, volume density and size (4 weeks: Control, 9; cMPC1$^{-/-}$, 9; 8 weeks: Control, 6; cMPC1$^{-/-}$, 12). Data are presented as mean ± SEM and analyzed by two-tailed unpaired Student's t-test.

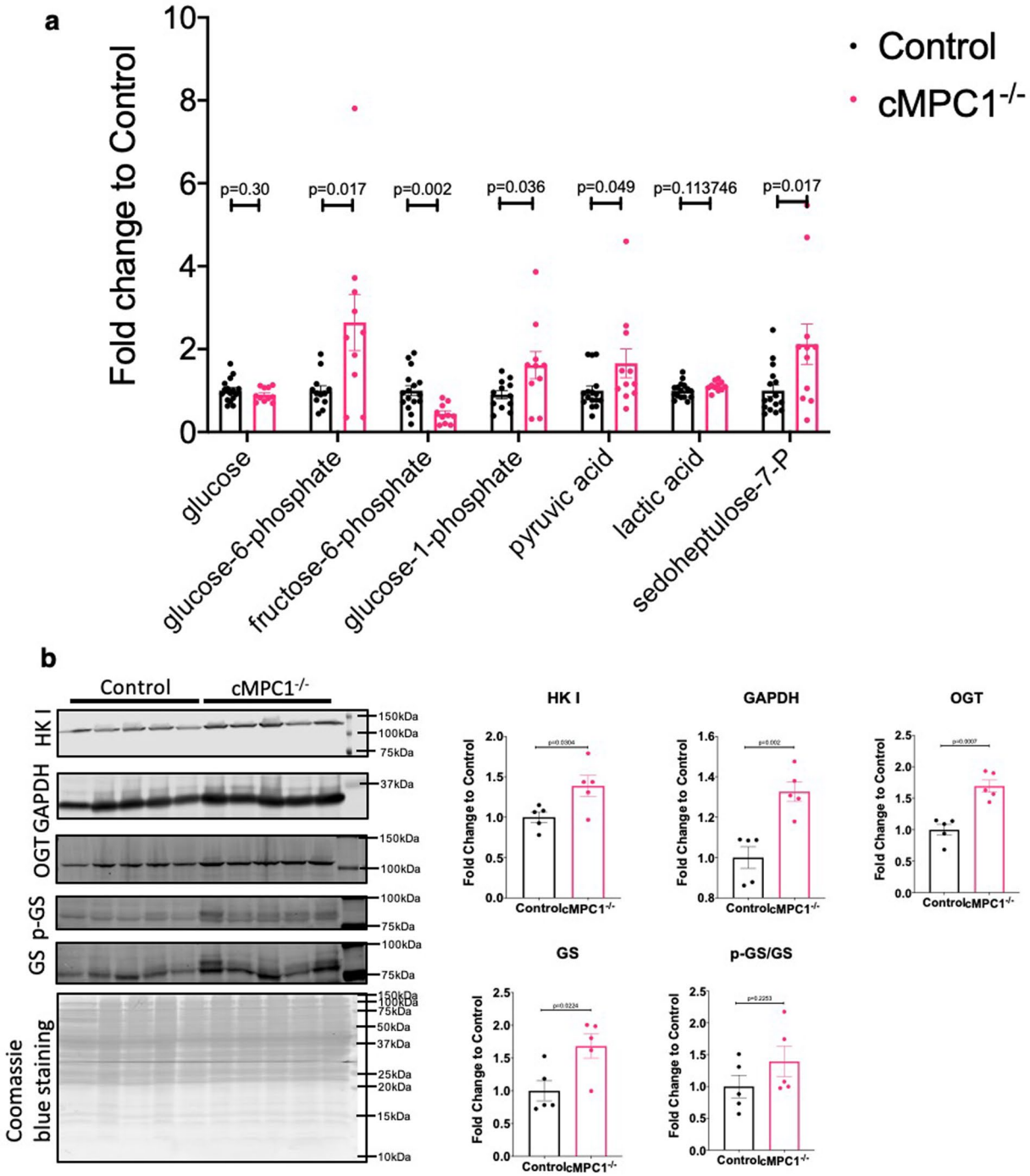

Extended Data Fig. 2 | Glycolysis enzymes and intermediates in cMPC1$^{-/-}$ hearts. a, Glycolysis-derived metabolic intermediates in 8-week-old control and cMPC1$^{-/-}$ hearts were determined by GC-MS. Mice were random fed before sacrifice. (Control, 15; cMPC1$^{-/-}$, 11). **b**, hexokinase I (HK I), GAPDH, O-GlcNAc transferase (OGT) and glycogen synthase (GS) blots were performed in lysates of cardiomyocytes isolated from 8-week-old control and cMPC1$^{-/-}$ mice. Protein quantification was normalized to total Coomassie blue staining. (n = 5 both groups). Data are presented as mean ± SEM and analyzed by two-tailed unpaired Student's t-test.

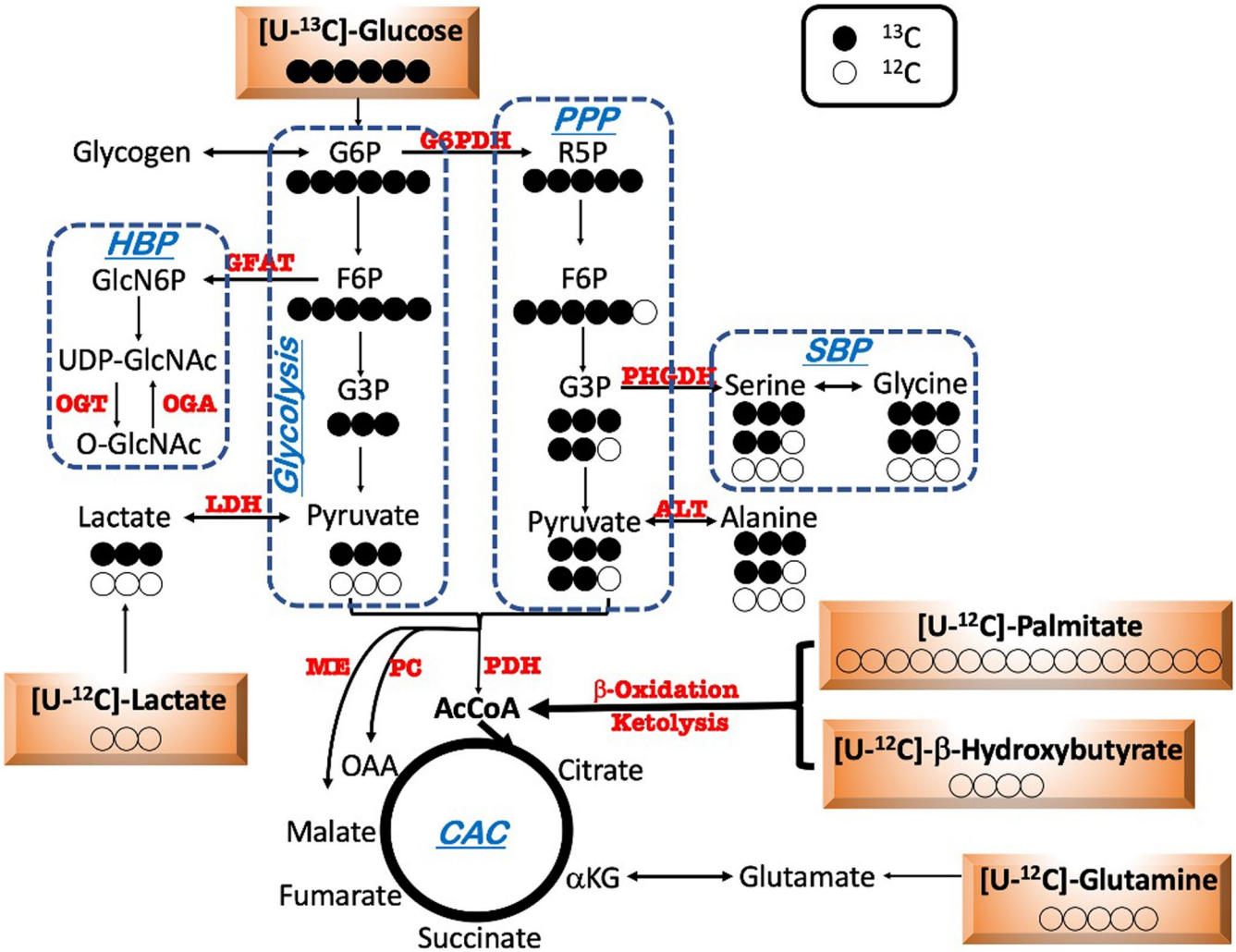

Extended Data Fig. 3 | Flux scheme of ^{13}C-labeled substrate utilization in cMPC1$^{-/-}$ hearts. Schematic depicting metabolic fate of uniformly labeled glucose ([U-$^{13}C_6$]-glucose) into glycolysis, the pentose phosphate pathway (PPP), serine biosynthesis pathway (SBP) and the Citric Acid Cycle (CAC). Closed and open circles represent ^{13}C-labeled and ^{12}C-labeled carbons respectively.

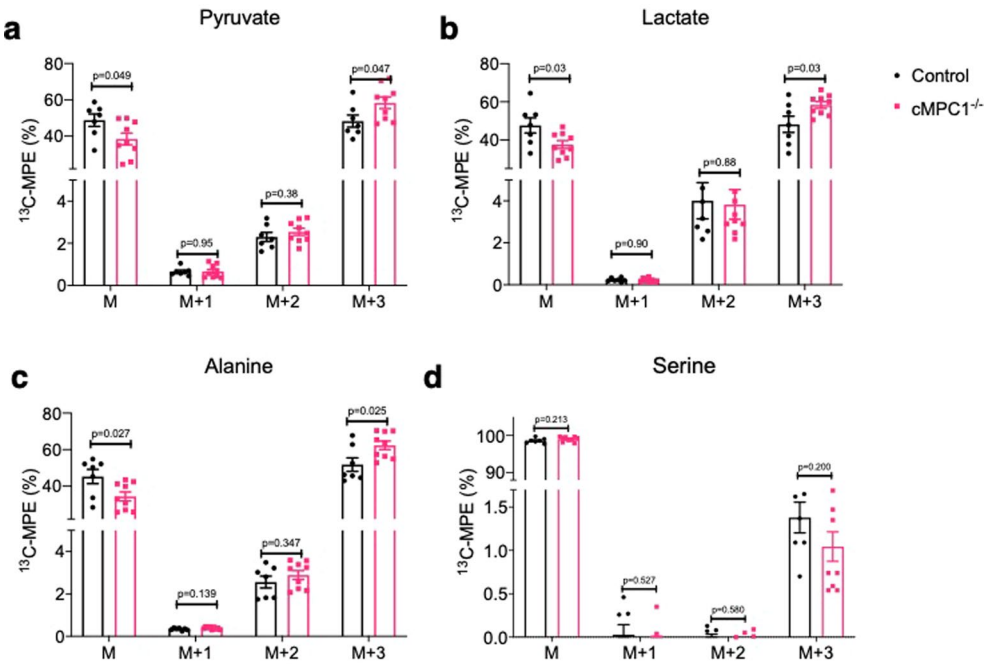

Extended Data Fig. 4 | ^{13}C-MPE for pyruvate, lactate, alanine and serine from [U-$^{13}C_6$]-glucose perfusion. ^{13}C-isotopomer labeling pattern of pyruvate (**a**), lactate (**b**), alanine (**c**) and serine (**d**) following [U-$^{13}C_6$]-glucose perfusion (Control, 7; cMPC1$^{-/-}$, 9). Data are presented as mean ± SEM and *P* values were determined by two-tailed unpaired Student's t-test.

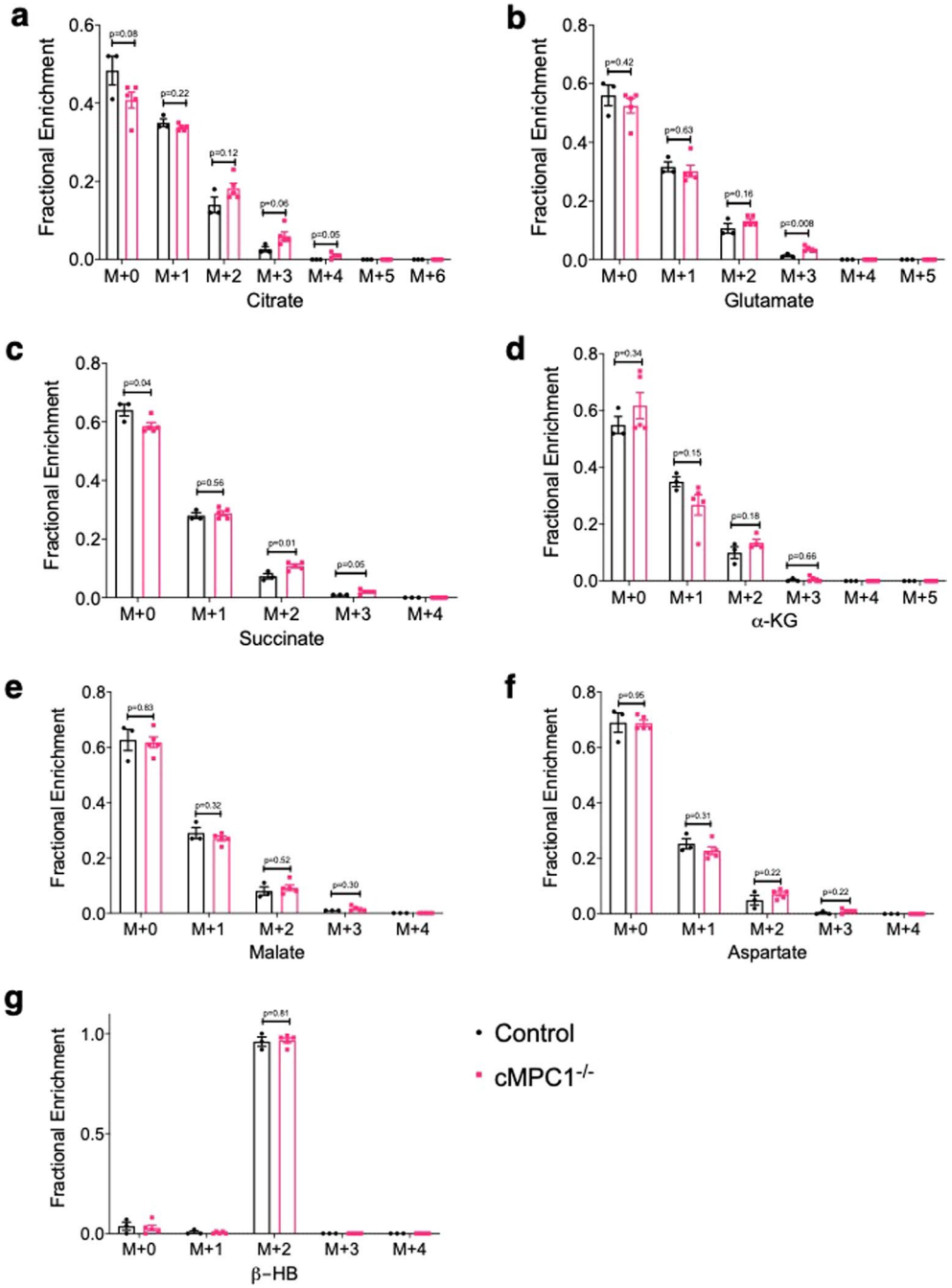

Extended Data Fig. 5 | ^{13}C-isotopomer labeling pattern of CAC intermediates from ^{13}C-β-HB perfusion. ^{13}C-labeled CAC intermediates analysis of Langendorff-perfused hearts perfused with [2,4-$^{13}C_2$]-β-HB and unlabeled glucose, palmitate and lactate. Fractional enrichment ^{13}C-labeled isotopomers of citrate (**a**), glutamate (**b**), succinate (**c**), α-ketoglutarate (KG) (**d**), malate (**e**), aspartate (**f**) and β-hydroxybutyrate (HB) (**g**) were determined by LC-MS (Control, 3; cMPC1$^{-/-}$, 5). Data are presented as mean ± SEM and *P* values were determined by two-tailed unpaired Student's t-test.

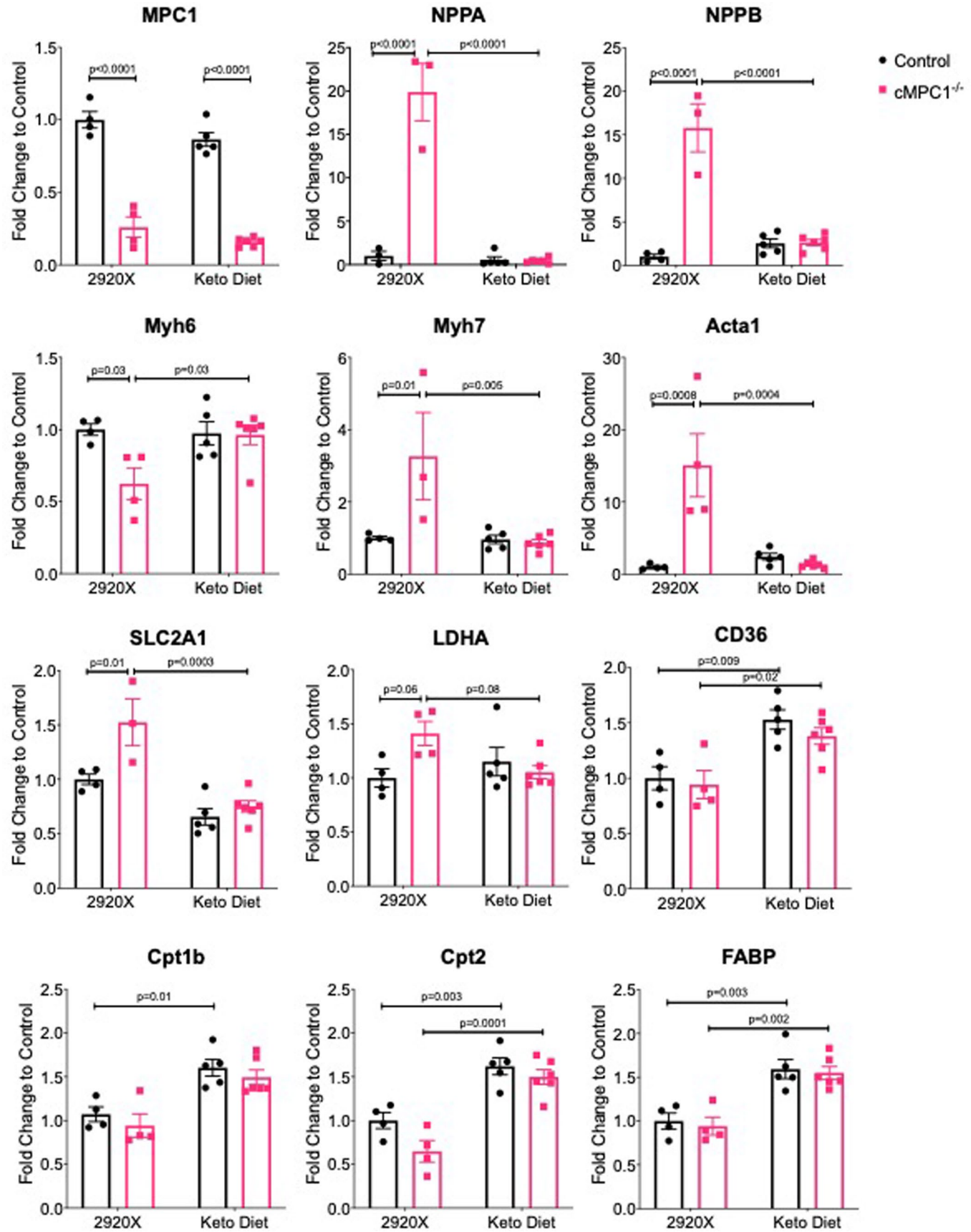

Extended Data Fig. 6 | Expression levels of hypertrophic markers and selected transcripts encoding metabolic genes in the cMPC1$^{-/-}$ hearts on 2920X and ketogenic diet. The cMPC1$^{-/-}$ mice under protocol 2 were analyzed for gene expression after 8-week-feeding on Ketogenic (Keto) Diet or control diet (2920X). Sample sizes: n = 4 (Control-2920X), n = 4 (cMPC1$^{-/-}$2920X), n = 5 (Control-Keto), n = 6 (cMPC1$^{-/-}$Keto). Data are presented as mean ± SEM and *P* values were determined by two-way ANOVA followed by Tukey multiple comparison test.

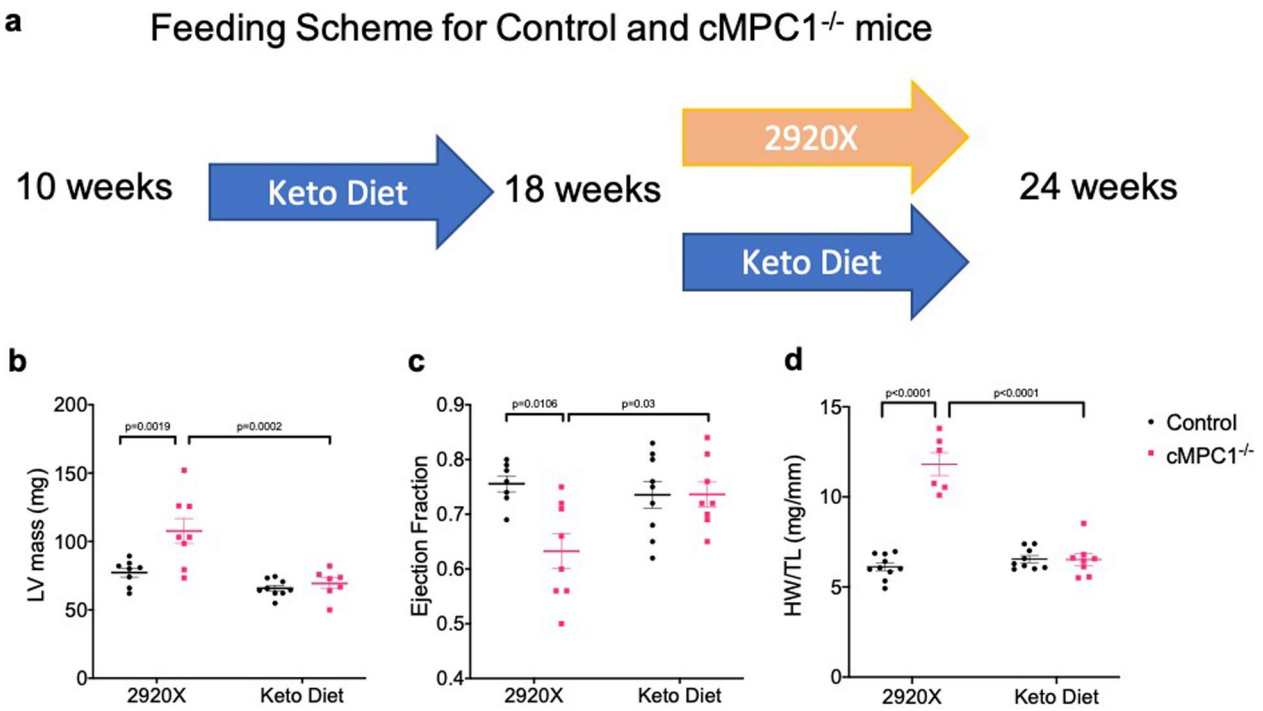

Extended Data Fig. 7 | Cardiac function of cMPC1$^{-/-}$ after switching ketogenic diet to regular chow. 10-week-old control and cMPC1$^{-/-}$ mice were fed a Keto Diet for 8 weeks and then 50% of mice of each genotype were switched to regular chow for 6 weeks. The feeding scheme is shown in panel (**a**). LV mass (**b**) and ejection fraction (**c**) were determined via echocardiography at the age of 22 weeks (4 weeks after chow switch). Heart weight and tibia length (**d**) was determined at the age of 24 weeks. Sample sizes: n = 10 (Control-2920X), n = 8 (cMPC1$^{-/-}$2920X), n = 9 (Control-Keto), n = 8 (cMPC1$^{-/-}$Keto). Data are presented as mean ± SEM and *P* values were determined by two-way ANOVA followed by Tukey multiple comparison test.

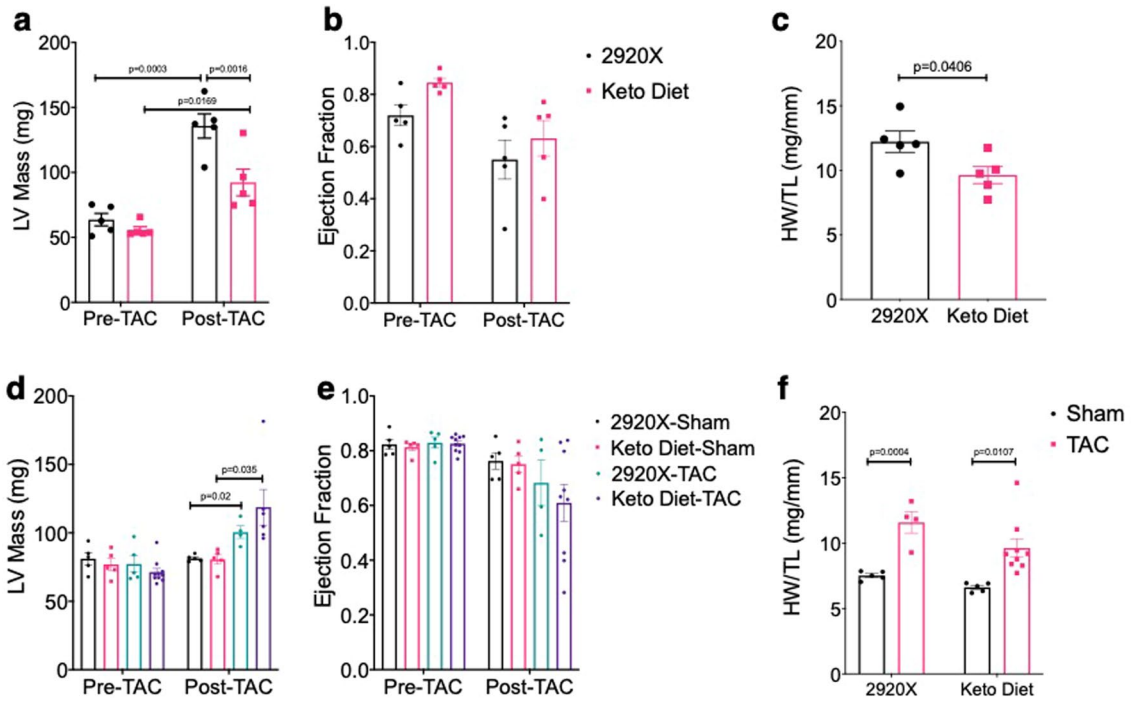

Extended Data Fig. 8 | Effects of ketogenic diet feeding on pressure overload-induced cardiac remodeling in WT mice. a–c, 8-week-old WT C57Bl6/J mice were fed with chow and Keto Diet 1 day before TAC surgery. LV mass (**a**) and ejection fraction (**b**) were measured by echocardiography prior to surgery and 3 weeks post TAC. Heart weight normalized to tibia length (**c**) was determined at the time of sacrifice. (n = 5 for both groups). **d–f**, 12-week-old WT C57Bl6/J mice were fed with chow and Keto Diet 1 day before sham/TAC surgery. LV mass (**d**) and ejection fraction (**e**) were measured by echocardiography prior to surgery and 3 weeks post TAC. Heart weight normalized to tibia length (**f**) was determined at the time of sacrifice. (n = 10 for Keto Diet-TAC group and n = 5 for other groups). Data are presented as mean ± SEM and *P* value was determined by two-way ANOVA followed by Tukey multiple comparison test.

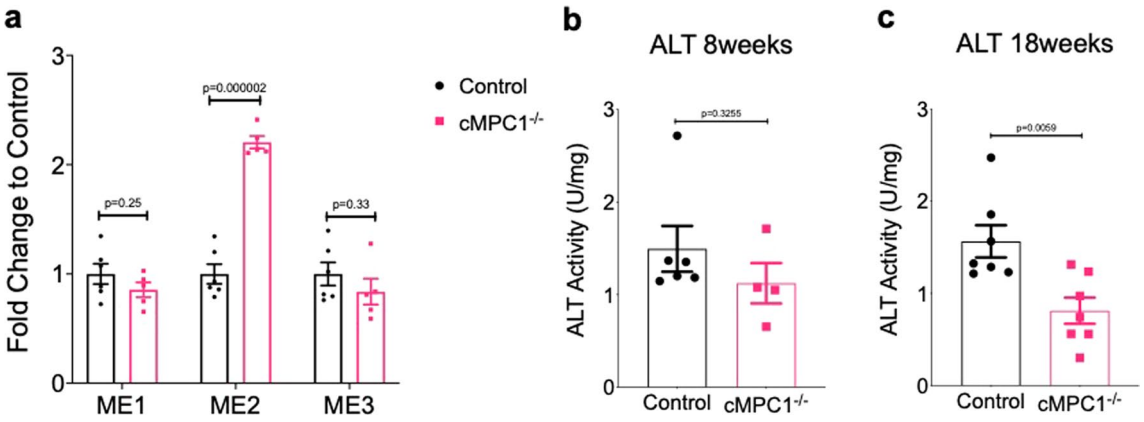

Extended Data Fig. 9 | mRNA level of ME isoforms and ALT activity in cMPC1$^{-/-}$ hearts. a, mRNA level of three malic enzyme isoforms were determined by qPCR in the hearts from control and cMPC1$^{-/-}$ mice (Control, 6; cMPC1$^{-/-}$, 5). **b**, **c**, ALT activity (Cayman 700260) were determined in the hearts from 8-week-old and 18-week-old control and cMPC1$^{-/-}$ mice (8-week-old group: Control, 6; cMPC1$^{-/-}$, 4. 18-week-old group: Control, 7; cMPC1$^{-/-}$,7). Data are presented as mean ± SEM and *P* values were determined by two-tailed unpaired Student's t-test.

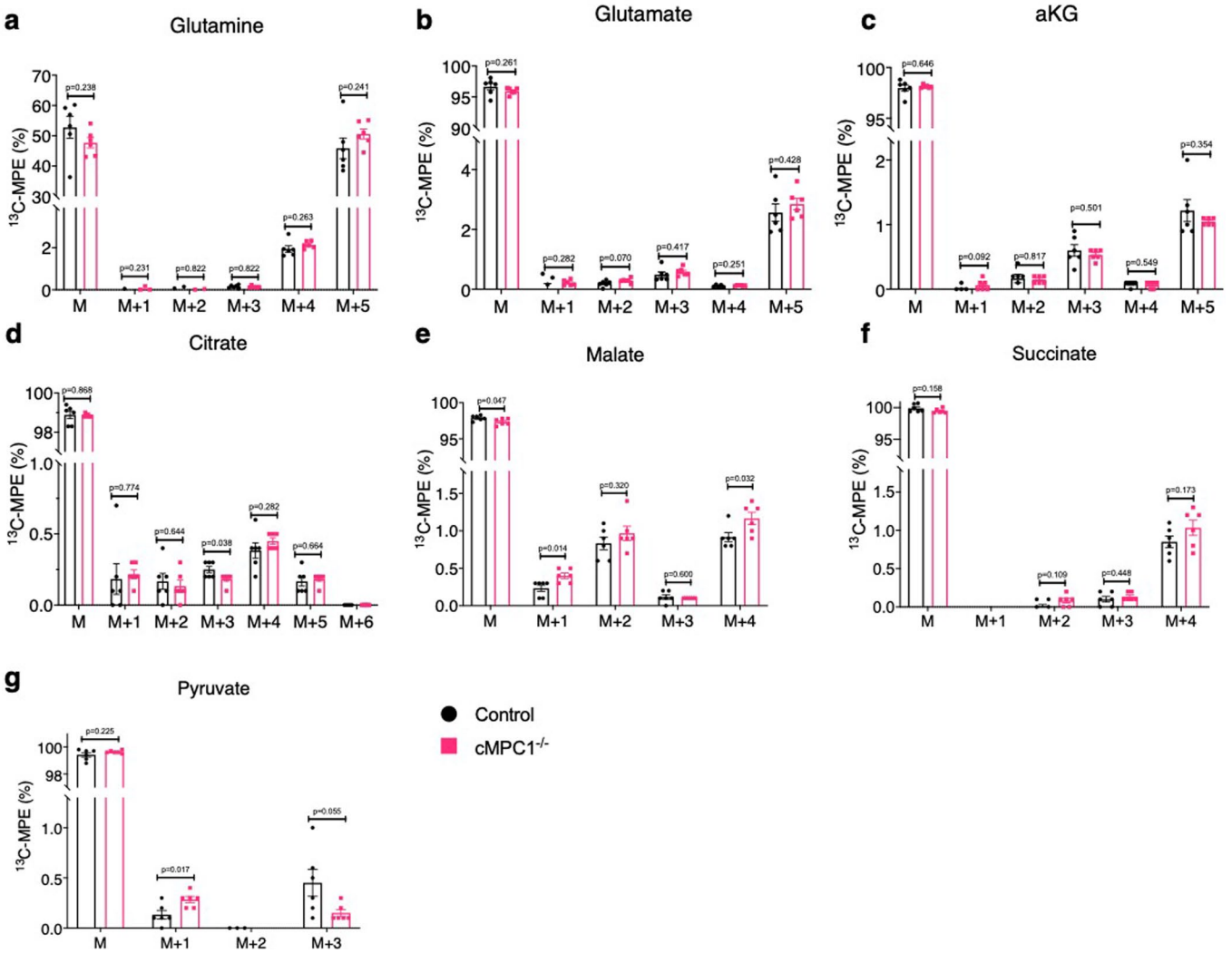

Extended Data Fig. 10 | ^{13}C-labeled CAC intermediates analysis from [U-$^{13}C_5$]-glutamine perfusion. ^{13}C-labeled CAC intermediates analysis of Langendorff-perfused hearts perfused with 0.5 mM [U-$^{13}C_5$]-glutamine and unlabeled substrates (10 mM glucose, 0.4 mM palmitate, 0.5 mM lactate, and 0.1 mM β-HB). ^{13}C-MPE of glutamine (**a**), glutamate (**b**), alpha ketoglutarate (a-KG) (**c**), citrate (**d**), malate (**e**), succinate (**f**) and pyruvate (**g**) were determined by GC-MS (Control, 6; cMPC1$^{-/-}$, 6). Data are presented as mean ± SEM and *P* values were determined by two-tailed unpaired Student's t-test.

nature research

Corresponding author(s): E. Dale Abel

Last updated by author(s): Jul 27, 2020

Reporting Summary

Nature Research wishes to improve the reproducibility of the work that we publish. This form provides structure for consistency and transparency in reporting. For further information on Nature Research policies, see Authors & Referees and the Editorial Policy Checklist.

Statistics

For all statistical analyses, confirm that the following items are present in the figure legend, table legend, main text, or Methods section.

n/a	Confirmed	
☐	☒	The exact sample size (*n*) for each experimental group/condition, given as a discrete number and unit of measurement
☐	☒	A statement on whether measurements were taken from distinct samples or whether the same sample was measured repeatedly
☐	☒	The statistical test(s) used AND whether they are one- or two-sided *Only common tests should be described solely by name; describe more complex techniques in the Methods section.*
☐	☒	A description of all covariates tested
☐	☒	A description of any assumptions or corrections, such as tests of normality and adjustment for multiple comparisons
☐	☒	A full description of the statistical parameters including central tendency (e.g. means) or other basic estimates (e.g. regression coefficient) AND variation (e.g. standard deviation) or associated estimates of uncertainty (e.g. confidence intervals)
☐	☒	For null hypothesis testing, the test statistic (e.g. *F*, *t*, *r*) with confidence intervals, effect sizes, degrees of freedom and *P* value noted *Give P values as exact values whenever suitable.*
☒	☐	For Bayesian analysis, information on the choice of priors and Markov chain Monte Carlo settings
☒	☐	For hierarchical and complex designs, identification of the appropriate level for tests and full reporting of outcomes
☒	☐	Estimates of effect sizes (e.g. Cohen's *d*, Pearson's *r*), indicating how they were calculated

Our web collection on statistics for biologists contains articles on many of the points above.

Software and code

Policy information about availability of computer code

Data collection	Echocardiography was performed using Vevo2100 (version 1.5). For isolated working heart perfusion, data was collected using LabChart (version 8.1.13). For in situ metabolomics, GC-MS and LC-MS data were collected using Xcalibur™ Software (version 4.1.31.9). Metabolite peak detection were performed by TraceFinder General Quant (version 4.1). For GC-MS on perfused hearts, data was collected using GC/MSD ChemStation Software (version E.02.02.1431). For LC-MS on perfused hearts, data was collected using Xcalibur™ Software (version 2.4.0.1824) and X13CMS R package (version 1.3). For NMR on perfused hearts, data was collected using TopSpin™ Software (version 4.0.3).
Data analysis	GraphPad Prism (version 8.3.1) was used for statistical tests. Cardiac fibrosis quantification was analyzed using ImageJ (version 1.51). In situ metabolomics was analyzed using MetaboAnalyst (version 4.0).

For manuscripts utilizing custom algorithms or software that are central to the research but not yet described in published literature, software must be made available to editors/reviewers. We strongly encourage code deposition in a community repository (e.g. GitHub). See the Nature Research guidelines for submitting code & software for further information.

Data

Policy information about availability of data

All manuscripts must include a data availability statement. This statement should provide the following information, where applicable:

- Accession codes, unique identifiers, or web links for publicly available datasets
- A list of figures that have associated raw data
- A description of any restrictions on data availability

Source data for western blots are provided with this paper. All other data that support the findings of this study are available from the corresponding author upon reasonable request.

Field-specific reporting

Please select the one below that is the best fit for your research. If you are not sure, read the appropriate sections before making your selection.

☒ Life sciences ☐ Behavioural & social sciences ☐ Ecological, evolutionary & environmental sciences

For a reference copy of the document with all sections, see nature.com/documents/nr-reporting-summary-flat.pdf

Life sciences study design

All studies must disclose on these points even when the disclosure is negative.

Sample size	No sample-size calculations were performed. All the experiments were performed using sample sizes based on standard protocol in the field and based on our previous studies. For detail sample size please see figure legends. Mol Cell Biol. 2014 Sep 15;34(18):3450-60. Journal of the American Heart Association (JAHA). 2013;2:e000301. Circulation Research Volume 122, Issue 6, 16 March 2018, 836-845 Journal of the American Heart Association (JAHA). Volume 8, Issue 17, 3 September 2019
Data exclusions	No data was excluded. The mice with health concerns including hydrocephalus, malocclusion and tumors were not used for data collection.
Replication	All experiments were performed independently. No attempts for replication failed.
Randomization	For special feeding experiment, both control and knockout mice were randomly assigned to different chow groups For TAC surgery experiment, both control and knockout mice were randomly assigned to sham or surgery groups. Mice used in all experiments were litter mate.
Blinding	All surgeries and echocardiography studies were carried out blinded to the genotype of the mice. For trichrome staining, fibrosis area quantification were analyzed by a researcher blinded to genotype.

Reporting for specific materials, systems and methods

We require information from authors about some types of materials, experimental systems and methods used in many studies. Here, indicate whether each material, system or method listed is relevant to your study. If you are not sure if a list item applies to your research, read the appropriate section before selecting a response.

Materials & experimental systems

n/a	Involved in the study
☐	☒ Antibodies
☒	☐ Eukaryotic cell lines
☒	☐ Palaeontology
☐	☒ Animals and other organisms
☒	☐ Human research participants
☒	☐ Clinical data

Methods

n/a	Involved in the study
☒	☐ ChIP-seq
☒	☐ Flow cytometry
☒	☐ MRI-based neuroimaging

Antibodies

Antibodies used	Primary antibodies used in Western blot: anti-MPC1 (Cell Signaling 14462); anti-MPC2 (Cell Signaling 46141); anti-O-linked N-Acetylglucosamine (Abcam ab2739); anti-VDAC (Cell Signaling 4661); anti-NDUFA9 (Abcam ab14713); anti-SDHA (Abcam ab14715); anti-UCR (Abcam ab110252); anti-MTCO3 (Abcam ab110259); anti-hexokinase I (Cell Signaling 2024); anti-GAPDH (Cell Signaling 2118); anti-OGT (Cell Signaling 24083); anti-glycogen synthase (Cell Signaling 3886); anti-phospho-glycogen synthase (Cell Signaling 47043). All primary antibody were diluted as 1:1000 in TBST. Fluorescence secondary antibody: Anti-rabbit IgG (H+L) (DyLight™ 680 Conjugate)(Cell Signaling, 5366); Anti-mouse IgG (H+L) (DyLight™ 800 4X PEG Conjugate) (Cell Signaling, 5257). Both secondary antibodies were diluted as 1:5000 in TBST.
Validation	MPC antibodies were validated by previous report: Cell Metab. 2015 October 6; 22(4): 669–681. All the other antibodies used in this study were validated by the vendor and through extensive use in other peer-review publications. For all the Western blots in this manuscript, all the primary antibodies were verified by the correct molecular weight on Western blot compared the protein ladder (Odyssey® One-Color Protein Molecular Weight Marker, 928-40000).

Animals and other organisms

Policy information about studies involving animals; ARRIVE guidelines recommended for reporting animal research

Laboratory animals	MPC1 floxed mice were provided by Dr. Eric B. Taylor and Dr. Jared Rutter (Cell Metab. 2015 October 6; 22(4): 669–681. doi:10.1016/j.cmet.2015.07.027). AlphaMHC-Cre transgenic mice were housed and used in Abel Lab for over 20 years (J Clin Invest. 1999;104(12):1703-1714). All experiments were performed on age-matched mice. For the 13C-labeled glucose perfusion experiment, only male mice were used; for all the other experiments, both male and female litter mates were used. The age of mice was 8 to 10 weeks unless specified in figure legends and manuscript.
Wild animals	The study did not involve wild animals.
Field-collected samples	The study did not involve samples collected from the field.
Ethics oversight	All protocols were approved by the Institutional Animal Care and Use Committee (IACUC) of University of Iowa.

Note that full information on the approval of the study protocol must also be provided in the manuscript.